

This item is the archived peer-reviewed author-version of:

Diatom frustule morphogenesis and function : a multidisciplinary survey

Reference:

De Tommasi Edoardo, Gielis Johan, Rogato Alessandra.- Diatom frustule morphogenesis and function : a multidisciplinary survey
Marine Genomics - ISSN 1874-7787 - Amsterdam, Elsevier science bv, 35(2017), p. 1-18
Full text (Publisher's DOI): <https://doi.org/10.1016/J.MARGEN.2017.07.001>
To cite this reference: <https://hdl.handle.net/10067/1445460151162165141>

1 **INVITED REVIEW**

2

3 **Diatom Frustule Morphogenesis and Function: a Multidisciplinary**
4 **Survey**

5

6 Edoardo De Tommasi ^a, Johan Gielis^b, Alessandra Rogato^{c,d*}

7

8 ^a Institute for Microelectronics and Microsystems, CNR, Via P. Castellino 111, 80131 Naples, Italy

9 ^b University of Antwerp, Department of Bioscience Engineering, Groenenborgerlaan 171, 2020

10 Antwerp, Belgium

11 ^c Institute of Biosciences and BioResources, CNR, Via P. Castellino 111, 80131 Naples, Italy

12 ^d Stazione Zoologica Anton Dohrn, Department of Integrative Marine Ecology, Villa Comunale 1, 80121
13 Naples, Italy

14

15

16

17 *Corresponding author:

18

19 Alessandra Rogato

20

21 Institute of Bioscience and BioResources, CNR,

22 Via Pietro Castellino 111, 80131 Naples, Italy

23 Tel.: +39 081 6132 410

24 Fax: +39 081 6132 706

25 e-mail: alessandra.rogato@ibbr.cnr.it

26

27

28

29

30

31

32

33

34

35

36

37

38 **Abstract**

39

40 Diatoms represent the major component of phytoplankton and are responsible for
41 about 20-25% of global primary production. Hundreds of millions of years of evolution led to
42 tens of thousands of species differing in dimensions and morphologies. In particular, diatom
43 porous silica cell walls, the frustules, are characterized by an extraordinary, species-specific
44 diversity.

45 It is of great interest, among the marine biologists and geneticists community, to shed
46 light on the origin and evolutionary advantage of this variability of dimensions, geometries
47 and pore distributions.

48 In the present article all the main results related to frustule morphogenesis and
49 functionalities with contributions from fundamental biology, genetics, mathematics, geometry
50 and physics are reviewed.

51

52

53

54

55 **Keywords**

56

57 Diatoms; frustule; genomics; Gielis superformula; biophysics.

58

59

60

61

62

63

64

65 **1. INTRODUCTION**

66

67 *“Few objects are more beautiful than the minute siliceous cases of diatoms: were they only created to be admired*
68 *under the microscope?”* [Darwin, Charles. On the Origin of Species by Means of Natural Selection. J. Murray,
69 London, 1859]

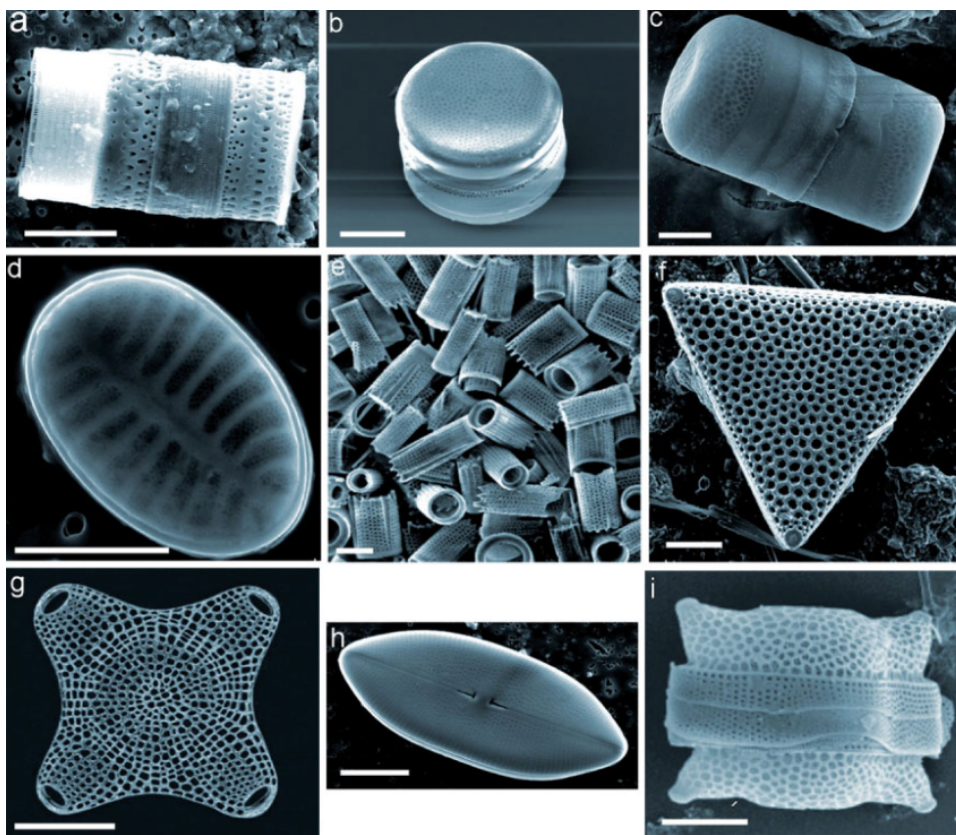
70

71 In the latter half of the nineteenth century, German naturalist Ernst Haeckel proposed
72 a kingdom, called Protista, composed of eukaryotic organisms that are not animals, plants nor
73 fungi and proposed a link between ontogeny (development of form) and phylogeny
74 (evolutionary descent). Furthermore, he developed the theory of non-random form, which
75 culminated in the beautifully illustrated *Kunstformen der Natur* (Art forms of nature) (Niklas
76 and Kutschera, 2016).

77 Among the classes belonging to Protista, he described also diatoms, phytoplanktonic
78 unicellular organisms included in the Stramenopila group, which are part of the supergroup
79 Chromalveolates, a completely separate evolutionary lineage from land plants (Katz, 2012). In
80 the Cretaceous, around 100 million years ago, diatoms began to become widespread and
81 developed great diversity (Gross, 2012). They are indeed one of the most diverse groups of
82 eukaryotes (Kooistra and Medlin, 1996) and estimates suggest that there are well over 250
83 genera and about 10^5 marine and freshwater species (Mann and Vanormelingen 2013). These
84 microalgae have the ability to generate a highly ornamented, fanciful and elegant porous silica
85 cell wall, known as the frustule. These cell walls exhibit an amazing diversity of species-
86 specific shapes and pore patterns, which made diatoms very popular organisms for
87 microscopist community in the Nineteenth century. The intricate structure of frustules was
88 used, indeed, to assess the quality of microscope optics (Round et al., 1990). Even nowadays,
89 high magnification images of diatom walls continue to amaze with their huge variety of micro

90 and nano-structures (Volcani et al. 1981) (Fig. 1). In addition, the silica cell walls produced by
91 diatoms give these single-celled algae a distinct and influential role in the ecology and
92 biogeochemistry of the oceans. Diatom silicification links the marine carbon and silicon
93 cycles: they are among the most productive organisms on earth, responsible for an estimated
94 20% of global primary production, and a corresponding 240 Tmol of annual biogenic silica
95 precipitation (Falkowski and Raven, 2007).

96

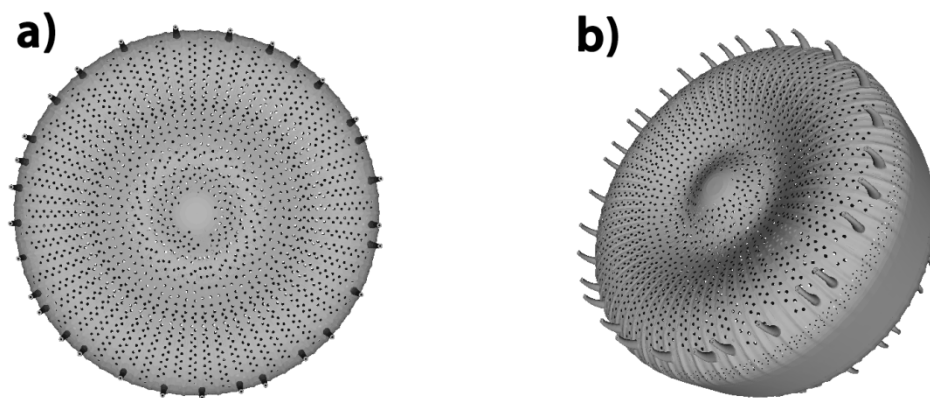


97

98 **Fig. 1.** Diatom shape diversity. Scanning Electron Microscopy (SEM) images of diatom frustules (a-d; f-i)
99 and fossilized diatom biosilica (e). Scale bar: 10 μm . Reproduced with permission from Losic et al., 2007.

100 A first distinction among diatoms traditionally starts from the symmetry of their
101 frustules: *Centric* or *Centrales* diatoms are characterized by a frustule with radial symmetry,
102 and are typically planktonic. *Pennates* diatoms have bilaterally symmetric frustules and are
103 mainly found in benthic and epipelagic communities (Round et al., 1990). In both cases, diatom
104 frustules resemble a petri-dish-like silica box, with a *hypotheca* inserted in a slightly bigger

105 *epitheca*, enclosing the living cell (Fig.2). The size of the frustule is species-dependent, and
106 varies from a few microns to millimeters. Both the *hypotheca* and the *epitheca* can be viewed
107 as a valve surrounded by a lateral girdle. Valves are made of several layers (*foramen*, *cribrum*
108 and *cribellum*), each provided with more or less regular patterns of pores, whose dimension
109 (from micron down to nanometer scale) and spatial distribution is species- and layer-specific.
110



111
112

113 **Fig. 2.** Schematic front (a) and angled (b) view of a CAD replica representing a generic *Stephanodiscus*
114 diatom frustule, provided with characteristic spines surrounding the valve.

115

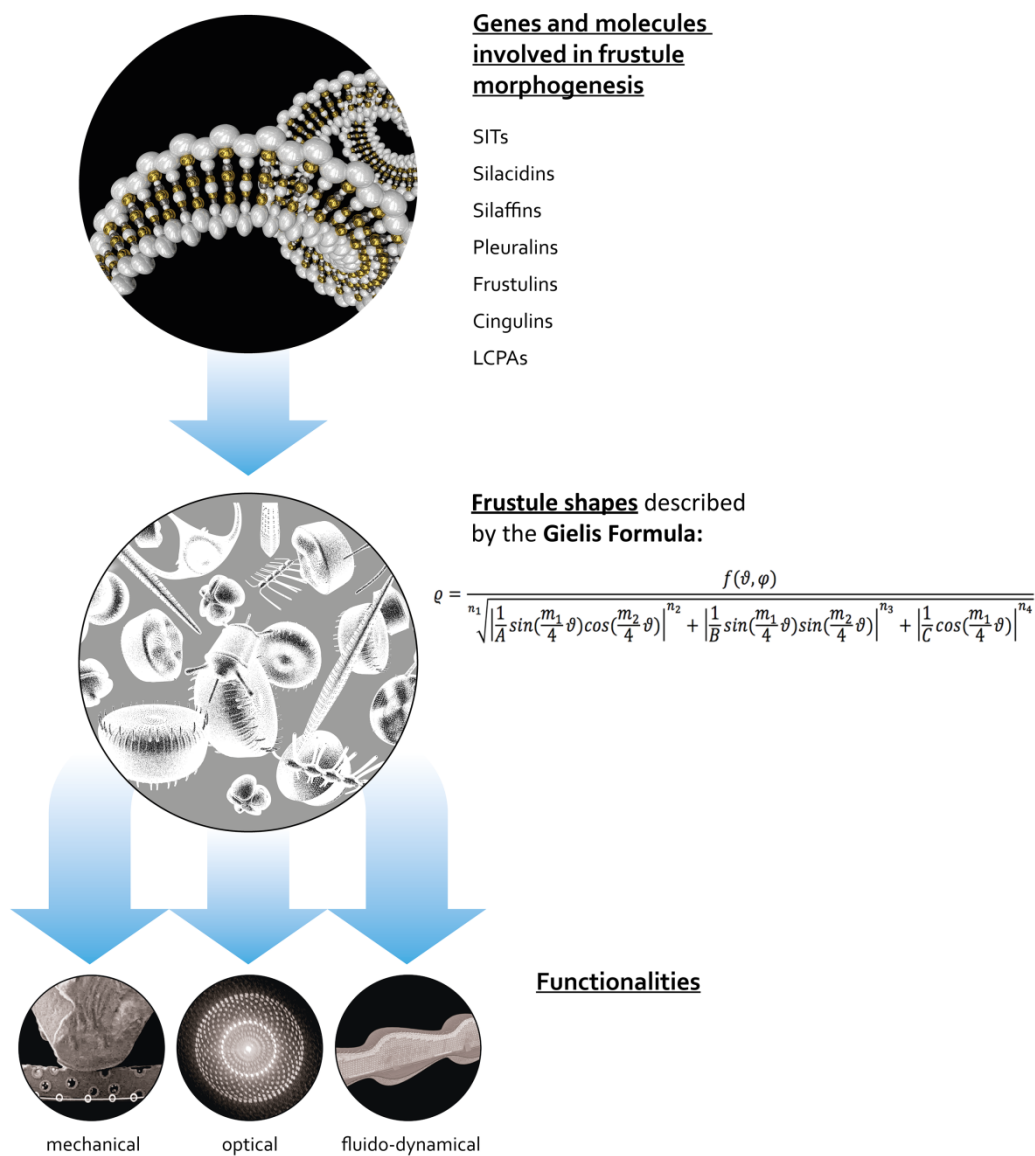
116 Diatom frustules are basically composed by hydrated, porous, amorphous silica
117 provided with several surface defects such as Si-OH (silanol) and Si-H groups (Qin et al.,
118 2008). An accurate analysis based on Raman and FTIR spectroscopies on frustules after
119 removal of the organic content allowed to detect also signals coming from organic residuals
120 incorporated in the porous matrix (mainly C-H bonds) and sporadic, localized signals from
121 sulfur composites (C-S and S-H bonds) (Kammer et al, 2010; De Tommasi, 2016). The
122 presence of sulfur residuals may be related to the global sulfur cycle, in which the role played
123 by phytoplankton is of fundamental importance, mainly through the release of
124 dimethylsulfide (DMS) in the atmosphere (Simó, 2001). Furthermore, frustules are

125 surrounded by extracellular polymers, mainly polysaccharides, whose functions comprise,
126 among others, sessile adhesion, gliding, protection against drying, and formation of biofilms
127 and colonies (Svetličić et al., 2013).

128 Through the years, applications of diatom frustules have gone far beyond microscope
129 quality testing. Beside the use of fossilized diatom biosilica (the so called *diatomite* or
130 *diatomaceous earth*) in toothpaste, facial scrubs and water filtration, recently the physical
131 properties of frustules found applications in several fields of micro-, nano- and bio-
132 technology. For example, frustules of centric diatoms have been successfully used as
133 microlenses (De Stefano et al., 2007; De Tommasi et al., 2010), being able also to squeeze light
134 under diffraction-limit (De Tommasi et al., 2014); their ability to collect light with high
135 efficiency can lead to the development of new generations of bio-based and bio-inspired solar
136 cells (Toster et al., 2013; Wang et al., 2013); metalized frustules have been successfully used
137 as nano-structured substrates in plasmonics (Payne et al., 2005; Ren et al., 2014; Kwon et al.,
138 2014); photoluminescence of frustules has been exploited in the realization of optical sensors
139 and biosensors (De Stefano et al., 2005; Gale et al., 2009); functionalized diatomite
140 nanoparticles can be used as vectors in drug-delivery (Terracciano et al., 2015; Delalat et al.,
141 2015); diatomite and frustules have been used as scatterers in random lasers (Lamastra et al.,
142 2014). Other interesting applications may come from a proper modification of the frustule:
143 metabolic insertion of germanium (Jeffryes et al., 2008) or titania (Jeffryes et al., 2008 bis)
144 allow to obtain efficient nanostructured semiconducting devices for optoelectronics,
145 enhanced light trappers in dye-sensitized solar cells and structured photocatalysts of toxic
146 chemicals; polymer (Losic et al., 2007 bis), silicon (Bao et al., 2007), or metallic (Fang et al.,
147 2012) frustule replicas can be used as masters for nanofabrications, in sensing and electronic
148 devices and as Enhanced Optical Transmission (EOT) plasmonic elements, respectively.
149 However, the most fascinating potentiality of diatom biosilica, which would lead to the

150 complete control of all the above mentioned applications and even more, relies on the ability
151 to manipulate the genes which rule frustule morphogenesis. Indeed we can imagine to modify
152 frustule morphology, geometry, shape and pore distribution in order to optimize a specific
153 application by mutating the proper genes (Kröger and Poulsen, 2008). Unfortunately the
154 genes involved in silica precipitation, aggregation, spatial rearrangement and relative
155 proteins are still not well characterized.

156 The diatom genome is a *mélange* of different genes, some resembling plants, others
157 animals or prokaryotes, which arose through successive endosymbioses and horizontal gene
158 transfers from bacteria (Bowler et al., 2008). The genetic and molecular details of frustule
159 morphogenesis have been partially elucidated only in recent years. Accurate knowledge of
160 diatom genome and genetics will help us to understand the processes that drive the
161 construction of the precise structure of frustules.



162

163 **Fig. 3.** Schematic representation of the interplay between genes and molecules, geometry and physics, pivotal to
 164 understand form, function and development.
 165

166

167 In this review we propose a link between morphology and functionalities of diatom
 168 frustules through a multidisciplinary approach which is schematized in Fig. 3. First, we will
 169 report the available informations of the genes putatively implicated in the machinery aimed at
 170 silica precipitation and frustule genesis, with a close examination of the known proteins,
 171 polyamines and other macromolecules involved in the process. Secondly, the most recent
 172 mathematical techniques for the description of natural shapes when subjected to given

173 constraints will give us the proper instrument to shed light on frustule diversity in shapes and
174 geometries, looking at it both as a whole and at its ultrastructure, down to pore dimensions
175 and arrangement. Finally, the main physical properties of frustules (mechanical, fluid
176 dynamical and optical), which represent the actual link between shape and functionality, will
177 be described.

178

179 **2. GENES AND MACROMOLECULES INVOLVED IN FRUSTULE MORPHOGENESIS**

180

181 Silicification in diatoms is a complex process, under strict genetic control. However,
182 although current techniques for genetic manipulation (Apt et al., 1996, Falciatore et al., 1999;
183 Poulsen et al., 2005 ; Kroth et al., 2007; De Riso et al., 2009; Niu et al., 2012; Daboussi et al.,
184 2014; Weyman et al., 2014; Sabatino et al., 2015; Karas et al., 2015 ; Hopes et al., 2016;
185 Rastogi et al., 2016) potentially allow to modulate the expression of the genes involved in
186 biomineralization in order to understand their impact on frustule structure, architecture and
187 functions, to date only few studies have been published on the genetic manipulation of
188 diatom silica forming machinery and none of them allows a functional characterization of
189 proteins regulating cell wall assembly (Knight a et al., 2016; Poulsen and Kröger, 2005;
190 Fischer et al., 1999).

191 In recent decades, a variety of organic and biological molecules have been
192 successfully separated and identified from cell-wall extracts. Most of the comprehensive
193 information available on genes and molecules involved in frustule formation and
194 morphogenesis comes from studies on few species, in particular *Thalassiosira pseudonana*
195 and *Cylindrotheca fusiformis* (Kröger et al., 1996; Kröger et al., 1999; Kröger and Poulsen
196 2007; Hildebrand 2008; Kröger and Poulsen 2008; Sumper and Brunner 2008, Matsukizono
197 and Jin, 2012; Lechner and Becker 2015). To date, many genomes from relevant pennate and

198 centric diatom species (e.g.: marine, freshwater, toxic, cold-water, and oleaginous) have been
199 sequenced and several others are in pipeline (Armbrust et al., 2004; Bowler et al., 2008;
200 Lommer et al., 2012; Trainer et al., 2012; Galachyants et al., 2015; Tanaka, et al., 2015; Traller
201 et al., 2016; Basu et al., 2017; Mock et al., 2017). The increased accessibility to whole genome
202 information from other diatom representative species have contributed to further understand
203 the mineralization process (Kröger and Poulsen 2007; Mock et al., 2008; Kröger and Poulsen,
204 2008; Scheffel et al., 2011; Shrestha et al., 2015; Durkin et al., 2016). Several research papers
205 and reviews have been published presenting the advances in the characterization of the
206 structure and function of diatom cell wall proteins and molecules. The following sections aim
207 to review and discuss the most recent knowledge on these molecules, the state of genetic
208 manipulation to modify frustule biosynthesis, the possible impacts of these manipulations on
209 cell wall and the molecular information generated by other -omics data (transcriptomics,
210 proteomics, metagenomics and metatranscriptomics) (Mock et al., 2008; Allen et al., 2008;
211 Keeling et al., 2014; Muhseen et al., 2015) in order to reveal the role and specificity of these
212 genes and molecules responsible for species shape.

213

214 *2.1 Silicon transporters (SITs)*

215 The most well characterized genes involved in biomineralization, encode the silicic acid
216 transporters (SITs), which transport silicic acid from seawater into the cell (Durkin et al.,
217 2016; Durkin et al., 2012; Shrestha et al., 2015; Thamatrakoln et al., 2006). Si (primarily in
218 the form of silicic acid, $\text{Si}(\text{OH})_4$) is actively taken from outside into the cell by the SITs. In
219 marine species, SITs are sodium-coupled active transporters with specific silicic acid uptake
220 activity, whereas in freshwater species there seems to be sodium and potassium coupled
221 transporters. These proteins were first identified and described by Hildebrand and coworkers
222 (Hildebrand et al., 1997) in the pennate *C. fusiformis*, and subsequently in all species studied
223 so far. Si transporter genes are constituted by several members, with differences in SITs

224 family size and functionality, that play different roles in the uptake of silicic acid with different
225 cellular localizations, Si binding affinities, and transport rates. Each SIT is predicted to contain
226 10 transmembrane domains (TMDs) and a coiled-coil motif at C-terminus. The mechanism by
227 which SITs recognize and bind silicic acid is still not completely known. Actually, a model has
228 been proposed in which a transport centered around the highly conserved GXQ amino-acid
229 sequence motif is hypothesized, directly involved in Si(OH)_4 binding (Hildebrand et al.,1998;
230 Thamatrakoln et al., 2006; Kröger and Poulsen, 2008; Marron et al., 2013; Lechner and
231 Becker., 2015; Knight et al., 2016). From an evolutionary point of view, the SITs genes
232 encoded by diatoms display sequence homology with proteins present in bacteria, most likely
233 acquired through horizontal gene transfer (Schroder et al., 2004; Ma et al., 2006 and 2007).

234 To better understand the origin and functional divergence of SITs proteins, Durkin and
235 colleagues in 2012 provided a comprehensive sequence-based analysis and more recently, in
236 2016, reconstructed a more exhaustive evolutionary scenario where SIT genes form five
237 separate clades, called A, B, C, D and E (Durkin et al., 2016), with Clade B at the basal position
238 within the clades . The idea is that SIT B proteins probably arose when the concentration of
239 silicic acid was around 1000 μM , orders of magnitude greater than today, suggesting that SIT
240 B proteins are involved in the passive transport to a specialized vesicle, called Silica
241 Deposition Vesicle (SDV), in high silicic acid environments. Moreover, the clade contains
242 proteins with amino acid residues that undergo post-translational modifications which can
243 affect the function of channel gating. On the contrary, proteins of SITs A, C, D and E clades, are
244 directly involved in the transport of silicic acid from the seawater to the SDV. SITs C and D
245 proteins have been found in all major diatom lineages whereas clades A and E are lineage-

246 specific with Clade A forming a monophyletic cluster, and including only sequences from
247 pennate diatoms. The functional diversification and specialization of SIT members might be
248 justified because diatoms, although unicellular organisms, may experience large differences
249 in silicon concentration between surface and deep water, between different oceanic regions
250 and between intracellular compartments (depending on the species). Diatoms developed
251 such efficient, fine and ultrafine structured uptake systems to provide a quick response to the
252 constant and rapid changes that take place in the ocean environment and that enable these
253 organisms to adapt to their environment and thrive (Maldonado et al., 1999; Frings et al.,
254 2016; Bhattacharyya and Volcani 1980; Shrestha et al., 2015; Frings et al., 2016; Durkin et al.,
255 2016; Martin-Jezequel et al., 2000). In order to clarify the specific role played by each gene,
256 fold change of SIT genes transcript studies involving different diatom species have been
257 conducted in different conditions. Recent research indicates that SITs protein expression is
258 closely related to the cell cycle, with a down regulation during cell division and consequent
259 cell wall synthesis. Analysis characterizing the knockdown mutants of the two major SITs in
260 *T. pseudonana* showed that the magnitude of this down regulation is inversely related to the
261 concentration of the silicic acid, suggesting for these transporters also a role in the sensing of
262 silicic acid levels, independently of the transport, that controls cell wall formation and
263 division process (Shrestha et al., 2015). Moreover, what remains still little known, is the
264 intracellular transport of silicic acid. Only recently, thanks to novel advances in molecular
265 tools, Knight and coworkers made a series of targeted mutations in *T. pseudonana* and *P.*

266 *tricornutum* SITs to further determine the location and function of the different proposed
267 conserved residues upon protein structure and function. In addition, they developed a new
268 method based on a fluorescent probe for silicic acid that will contribute to understand the
269 mechanisms of silicon transport *in vitro* (Knight a et al., 2016).

270 With the same purpose, Javeheri and colleagues introduced a mathematical model to
271 describe silicon dynamics in the diatom *T. pseudonana*, obtaining good agreement with
272 experimental data relative to silicon transport dynamics in four compartments: external
273 environment, cytoplasm, SDV and deposited silica (Javaheri et al., 2014). The hypothesis is
274 that the coordinated Si transporter actions underlie a flexible network that mobilizes Si in
275 response to many environmental changes and that these proteins are differentially regulated
276 at various levels. However an additional possibility is also a functional redundancy of these
277 transporters.

278 A more focused analysis on the reported profiles of expression of the different silicon
279 transporters in different diatom species will give new insights on the existence of a Si
280 transduction pathway involved in diatom biomineralization, cell cycle and growth mediated
281 by these proteins. A full comprehensive description of all SITs functions and evolution is
282 beyond the scope of this review, but it has to be highlighted that only through a functional
283 characterization it will be possible to identify the independent and specific and/or synergistic
284 and/or redundant activity of the individual carriers.

285

286 *2.2 Frustulins, Silaffins, Silacidins, Pleuralins and Cingulins*

287 Beside transport, diatom morphology is controlled by additional protein families
288 required for silica precipitation and molecules working as cell wall scaffold (Durkin et al.,
289 2012; Scheffel et al., 2011; Wenzl et al., 2008; Kröger and Poulsen, 2008; Kröger et al., 1999;

290 Kröger et al., 1996). Silica precipitation and polymerization occurs in a very ordered way;
291 after uptake, silicon is transported to the SDV, that contains silica forming organic
292 components, where silica formation takes place (Poulsen et al., 2013).

293 Over the last 20 years, significant progress has been made in the identification and study of
294 many of these proteins. Herein we review the most advances in the knowledge of
295 their functions.

296 The first protein was isolated from the cell wall of the diatom *C. fusiformis* (Kröger et al.,
297 1996) and called frustulin. Later on, these glycoproteins have been identified in different
298 diatoms species, both centric and pennate and all are characterized by the presence of a
299 conserved large cysteine-rich domains domain (acidic and cysteine-rich domains ACR) and a
300 species specific C-terminus. Frustulines are, amongst the protein families involved in silica
301 formation, the only that are present across the cell wall. This suggests that they have a role in
302 protection of the frustule rather than in its biogenesis (Kröger and Poulsen, 2008; van de Poll
303 et al., 1999).

304 Whereas frustulines do not play an active role in silica formation, silaffins, silacidins,
305 pleuralins and cingulins, are strictly confined to the silicalemma and are known as silica-
306 forming proteins (Wenzl et al., 2008; Scheffel et al., 2011). These proteins have enzymatic
307 activity and promote polymerization and deposition of silica from inorganic precursors. They
308 contain common amino acid motifs (e.g., lysine-rich), and are derived from precursor
309 polypeptides containing N-terminal signal peptides for import into the endoplasmic reticulum
310 (ER) (Kröger et al., 1999; Kröger et al., 2002; Sumper and Kröger, 2004; Pamirsky et al.,
311 2013;).

312 Silaffins, whose name derives from their high affinity to silica, have the capacity to
313 initiate and modulate silicon dioxide precipitation. Silaffins are able to precipitate silica *in*
314 *vitro*, forming spheres or plates containing regularly distributed nano and micro pores

315 (Kröger et al., 2002; Pamirsky et al., 2013). The primary structure of a precursor of silaffins
316 was isolated in *C. fusiformis* (Kröger et al., 2002), and later other genes have been found in
317 different diatom species. All the silaffins identified so far lack any sequence conservation but
318 all are rich in serine and lysine, and are subjected to different post-translational modifications
319 during intracellular maturation. These are essential for SDV and silica targeting and necessary
320 for the formation of silicon dioxide (Kröger and Poulsen, 2008; Kröger et al., 1999).

321 Pleuralins are protein components associated with the pleural bands, the region of
322 overlap between the two valves of the frustule. Pleuralines are not encoded in all the genomes
323 sequenced thus far. However, and only recently, it has been reported in *C. fusiformis* that the
324 role of pleuralins could be to bind simultaneously silaffins and frustulins , in order to connect
325 epi and hypotecha at the girdle bands (Kröger and Poulsen, 2008, De Sanctis et al., 2016).

326 The silacidins play a structural role in diatom frustules and, like silaffins, are
327 phosphorylated and the high degree of phosphorylation of the serine residues is strictly
328 related to their ability to precipitate silica nanospheres (Richthammer et al., 2011).

329 Recently, Kröger and coworkers reported the discovery of a new class of proteins in several
330 diatom species that contrarily to sillaffins and silacidins appear to be crucial in the molecular
331 mechanisms of silica assembly (Scheffel et al., 2011). In particular, these proteins seem to be
332 involved in the morphogenesis of the girdle band, also termed *cingulum*, and for this reason
333 are called cingulins.

334 For none of the aforementioned genes functional characterization is reported in literature. A
335 joint analysis of the available transcriptomic and proteomic data can provide useful insights
336 in their functions and regulation in order to build dynamic models connecting gene function
337 with biomineralization processes.

338

339

340 *2.3 Other frustule-related molecules*

341 Long-chain polyamines (LCPAs) are linear polyamines constituting the main organic and
342 soluble fraction of the biosilica matrix in all diatoms studied to date. As for the majority of the
343 frustule related molecules, LCPAs have been identified and isolated in the diatom *C. fusiformis*
344 (Kröger et al., 1997 and 2001) and, like silaffins and silacines, are able to precipitate silica *in*
345 *vitro*. Before their identification in diatom frustules, LCPAs have been identified almost
346 exclusively in bacteria and archaea, predominantly in extremophiles. Interestingly, in diatoms
347 they display species-specific differences in degree of methylation, chain length and position
348 of secondary and tertiary amines (Sumper and Brunner, 2008; Bridoux and Ingalls, 2010;
349 Gräb et al., 2016). This suggests that they may be directly responsible for the differences in
350 the nanopatterned biosilica frustule across different diatom species (Poulsen and Kröger,
351 2004; Sumper and Lehmann, 2006; Scheffel et al., 2011; Bridoux and Ingalls, 2010). Recently,
352 Gräb and coworkers proposed a model in which LCPAs interact with the lipid membrane of
353 the SDV and play a role in the control of expansion process of the SDV during cingulum and
354 epi – and hypo-theca formation (Gräb et al., 2016).

355 Another compound embedded within the frustule is chitin, a structural polysaccharide that
356 contributes to the rigidity of the cells. Chitin represents the most abundant polymer in the
357 ocean widely distributed among eukaryotes, archaea and bacteria and its biosynthesis
358 requires a set of multiple chitin synthase (CHS) genes encoded by multi-copy gene family.
359 CHSs genes have been found in different diatom species, and
360 molecular phylogenies reveal five separate clades (Brunner et al., 2009; Durkin et al., 2009).
361 Chitin does not seem involved in silica deposition directly, but rather it seems to direct the
362 correct layout of the proteins involved in biomineralization (Richthammer et al., 2011). The
363 exact mechanism by which chitin is assembled and the way it interacts with the components
364 of the frustule are still not known. However, transcriptome analysis of the Si and Fe response

365 in *T. pseudonana* reported an increased expression of two genes encoding chitin-binding
366 proteins, p150 and p150-like, an overproduction of chitin and a consequent elongated cell
367 phenotype with a tendency to aggregate and sink. This suggests that chitin may also play a
368 role in signalling and response to changes in environmental conditions, influencing cell wall
369 morphology and/or assembly and inducing a survival strategy for cells in hostile
370 environments (Durkin et al., 2009 and 2012).

371

372 *2.4 Frustule composition influenced by nutrient availability*

373 The different frustule related genes and molecules involved in silica formation and
374 composition, are influenced by different environmental constraints such as nutrient supply
375 and light intensity. Likewise, frustule structure and architecture influence nutrient uptake and
376 light perception (Mock et al., 2008; Allen et al., 2008; Soler et al 2010; Knight et al., 2016).

377 Some examples are shown of how Si concentration and availability, together with
378 other macronutrients such as carbon (C), nitrogen (N), phosphorus (P), and iron (Fe), could
379 limit diatom growth and division, affect diatom physiology and the mechanical properties of
380 frustules influencing the genes and genes products involved in diatom silicification
381 (Brzezinski et al., 2008).

382 In 2008, Mock and coworkers (Mock et al., 2008) and later, in 2012, Shrestha and
383 coworkers (Shrestha et al., 2012), reported a genome-wide transcriptome analysis of the
384 marine diatom *T. pseudonana*, experimentally identifying a direct molecular interaction
385 between Si and Fe metabolism and frustule related genes expression. To examine which of
386 these gene products may be involved in silicification pathways, the authors constructed a
387 comprehensive gene expression array. Findings from the two studies revealed that nutrient
388 availability either up- or down-regulate the expression of genes involved in silicification, in
389 particular the SITs, in agreement with previous reported results, showing increased silicon

390 cellular content in response to Fe, N and P limited growth conditions. Consequently, the
391 increased Si content, due to the altered stoichiometry of Si to C- and N- ratios, results in a
392 thicker and mechanically stronger frustule that makes cells less susceptible to grazers (Wilken
393 et al., 2011; Bucciarelli et al., 2010; Mock et al., 2008; Claquin et al., 2002). Moreover, in N and
394 P starved cells an accumulation of lipids in the frustule fraction has been reported, which
395 could impact the frustule architecture (Soler et al., 2010; Smith et al., 2016). In addition, a
396 silica-dependent checkpoint in diatom cell cycle progression has been demonstrated. During
397 their vegetative reproduction, diatoms need to build up a new silica cell wall, but if the
398 amount of silicon in the environment is depleted, cell division arrests in the G1-phase or G2-M
399 phase (Okita and Volcani 1980; Thamatrakoln et al., 2007; Bowler et al., 2010; Huysmann et
400 al., 2014; Tanaka et al., 2014). Finally, Durkin and collaborators in 2012 extended the
401 transcriptional analysis of genes encoding SITs, chitin synthases, and proteins involved in
402 silica formation in response to nutrient starvation in natural populations. Their results
403 highlight the important role of nutrient availability in frustule-related gene transcription and
404 consequently in shaping diatom community composition (Durkin et al., 2012).

405 All together these data clearly have a profound ecological significance and could help to
406 explain the large-scale ecological success of diatoms, suggesting the existence of an intimate
407 crosstalk between different processes interacting with each other and working in
408 collaboration to respond and adapt to multiple environmental factors and conditions.

409

410 **3. DIATOMS AS MODEL SYSTEMS FOR GEOMETRY**

411

412 *3.1. A generalized Pythagorean Theorem for the uniform description of algae*

413 Ultimately the shape of the frustules, the structure of valves and girdles, and the
414 distribution of pores need to be studied via mathematics, with emphasis on geometry,

415 optimization and energy minimization. In particular, there is a need for a dedicated
416 geometrical structure. There are many applications of mathematics in biological sciences,
417 especially in computational genomics. Genes and genetics are important factors in
418 development and evolution, but it can be argued that first and foremost organisms have to
419 abide to physical and mathematical laws, globally and locally. A problem is that biology, in
420 general, does not have laws like physics has, apart from allometric laws (Dhar and Guiliani,
421 2010; Niklas, 2004). To achieve the well known unreasonable effectiveness of mathematics in
422 the natural sciences, which is in that case in physics, seems a formidable task. The
423 mathematician I. M. Gelfand wrote: *"There exists yet another phenomenon which is*
424 *comparable in its inconceivability with the inconceivable effectiveness of mathematics in*
425 *physics noted by Wigner - this is the equally inconceivable ineffectiveness of mathematics in*
426 *biology"* (Arnold, 1999). Currently mathematical or geometrical models or laws to describe
427 trajectories of biological organisms through their lifetime or spacetime are simply not
428 available (Berger, 2003).

429 A geometrization of biology, or more generally of nature, based on forms and
430 formation of natural shapes (a geometrical theory of morphogenesis) is both an enormous
431 challenge and a prerequisite for progress in science and the life sciences. What needs to be
432 achieved is the combination of a uniform description of shapes, coupled to differential
433 equations within a coherent geometrical framework. This is exactly how physics evolved, with
434 the laws of gravitation based on a uniform description using circles, based on the Pythagorean
435 Theorem, or using conic sections, based on the Pythagorean application of areas. Later the
436 geometrical setting became Riemannian geometry and increasingly Finsler geometry with
437 applications in marine biology (Antonelli and Miron, 2013). Only with a uniform description
438 for biological shapes, the laws that govern shape and morphogenesis can be found, and only
439 then biology can deal with form and function of biological organisms, in the same way physics

440 has achieved. What is needed then is first, a uniform description of natural shapes (the
 441 Kepler-like step, May), and second, the study of the biological organisms in their ever-
 442 changing environment and the way they deal with stresses and curvatures.

443 Gielis Transformations are generic geometric transformations of planar functions $f(\vartheta)$,
 444 which unify a wide range of natural and abstract shapes (Gielis 2003 and 2017; Gielis et al.,
 445 2005). Equation 1 is a generalization of the circle (as a constant function) but it retains the
 446 compact structure of the Pythagorean Theorem: indeed, selecting $n_1 = n_2 = n_3 = 2$ and
 447 $f(\vartheta) = R = 1$ gives the unit circle and the Pythagorean theorem. Instead of only the classic
 448 Euclidean circle, Eq.1 defines natural shapes at all levels, such as diatoms, starfish, flowers
 449 and molluscs (Gielis 2003 and 2017; Gielis et al., 2005), as well as regular polygons
 450 (Matsuura, 2015), and even spacetime models (Gielis et al., 2005). The exponents $n_{1,2,3}$
 451 change the basic polygons defined by the symmetry parameter m . Parameters A and B are
 452 scaling parameters. If $A = B$, the basic shape is a circle, but when they differ, the basic shape is
 453 an ellipse. Since shape and size parameters are real numbers, a huge diversity and variability
 454 can be described in a very compact way:

$$455 \quad \varrho(\vartheta, f(\vartheta), A, B, m, n_1, n_2, n_3) = \frac{1}{\sqrt[n_1]{\left| \frac{1}{A} \cos\left(\frac{m}{4}\vartheta\right) \right|^{n_2} + \left| \frac{1}{B} \sin\left(\frac{m}{4}\vartheta\right) \right|^{n_3}}} \cdot f(\vartheta) \quad \text{Equation 1}$$

456 In particular, diatoms and their substructures can be described in one coherent
 457 framework (Figure 1). With $m=0$ (circle) radially symmetrical cylindrical frustules can be
 458 described, and with increasing m various diatom shapes are modelled (Fig. 1). Square shapes
 459 have $m=4$ and benthic diatoms with pennate shapes have bilateral symmetry, defined by $m=2$.
 460 *Stictodiscus* diatoms can be circular but also triangular ($m=3$) or square (Figs 1 and 4). Higher
 461 symmetries can be observed in sectorized *Arachnodiscus* or *Cosnicodiscus*. Actually, the
 462 parameter m divides the plane into m sectors. For $m=1$ the sector is 360° but unlike the circle,
 463 this shape can be asymmetrical, with one axis of symmetry. In algae, such asymmetry or

464 polarity is well known in establishment of polarity in *Fucus* or in zygotes of *Dictyota* (Bogaert
 465 et al., 2017), in oogonia (Fig. 6), or in the diatom *Podocystis*.

466 Equation 1 concerns planar curves, but the 3D version, Equation 2, a generalization of
 467 the sphere for $f(\vartheta, \varphi) = R$ (= the radius of the sphere), can describe the shape of the complete
 468 frustule:

469

$$\varrho(\vartheta, \varphi, f(\vartheta, \varphi), A, B, C, m_1, m_2, n_1, n_2, n_3, n_4)0$$

470

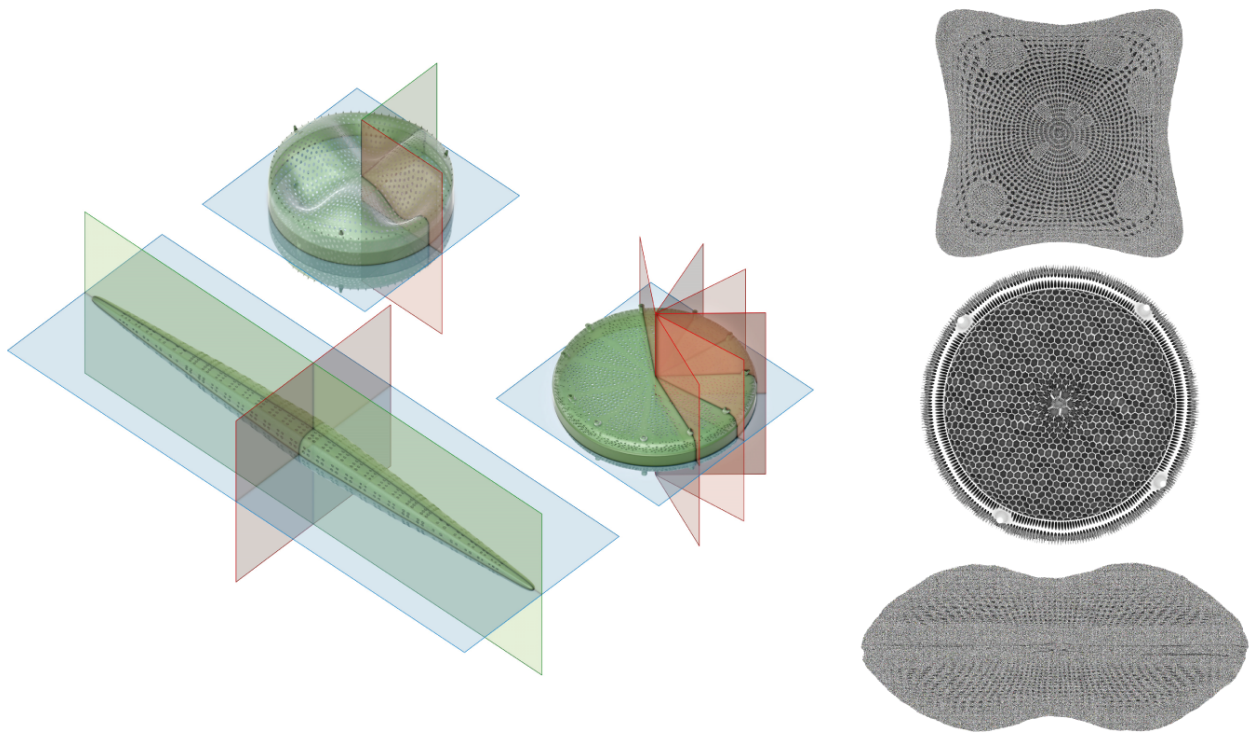
$$= \frac{1}{\sqrt[n_1]{\left| \frac{1}{A} \sin\left(\frac{m_1}{4}\vartheta\right) \cdot \cos\left(\frac{m_2}{4}\varphi\right) \right|^{n_2} + \left| \frac{1}{B} \sin\left(\frac{m_1}{4}\vartheta\right) \cdot \sin\left(\frac{m_2}{4}\varphi\right) \right|^{n_3} + \left| \frac{1}{C} \cos\left(\frac{m_1}{4}\vartheta\right) \right|^{n_4}}}$$

471

472 Equation 2

473

474



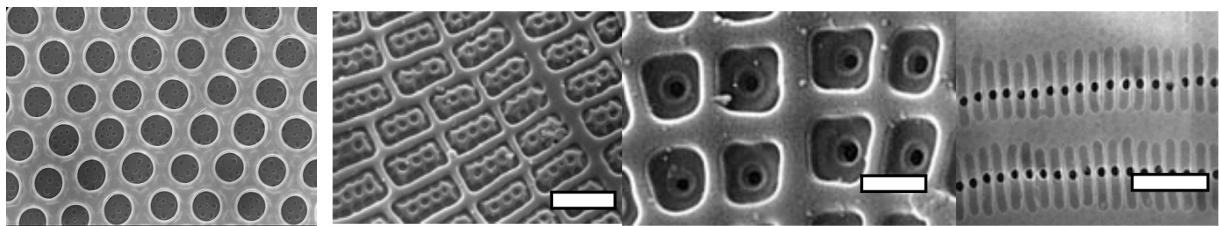
475

Fig. 4 Coordinate planes on CAD models (left) and Digital Diatoms (right; Courtesy of M. Kay, 2010)

476 The 3D coordinate planes then correspond to the valvar, radial/transapical and the
477 (per)apical planes in diatoms (Fig. 4). The arrangement of the pores in fact provides a very
478 specific coordinate system adapted to the shape, as a natural generalization of classical
479 coordinate systems such as spherical and elliptical coordinates. The regularity in the
480 distribution of pores is remarkable, both in centric and pennate diatoms, with local deviations
481 based on the actual processes in actual environmental conditions. Using the pores as a natural
482 coordinate system should then allow to understand the mathematical physics underlying
483 species specific and environmental-developmental specific distribution of pores.

484

485



486

487

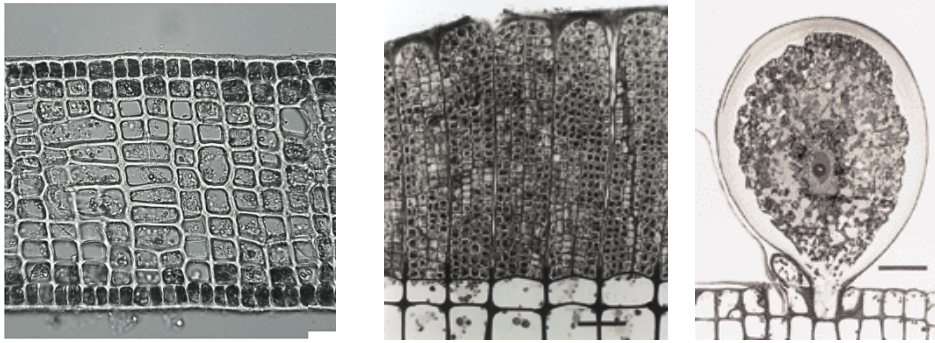
Fig. 5. Left: Pore distribution on *Coscinodiscus wailesii* valves. Right: Areolae array, microchambers and microchannels of *Cocconeis scutellum* vars. Scale bars 1.5 μ m (Courtesy of De Stefano et al., 2008, 2011).

488 In particular, every shape can be assigned its own set of parameters, allowing to deal
489 with phenoplastic variability, within single diatoms or among species and individuals, to any
490 desired degree of accuracy. The 'round' or 'square' shapes in Fig. 5, can be quantified
491 precisely and individually, using methods described for tree rings (Shi et al., 2015), bamboo
492 leaves (Lin et al., 2016) and seeds. It is noted that this geometrical strategy is far more general
493 than the geometrical ones used for automatic identification of diatoms, e.g. based on contour

494 shape analysis (Hicks et al., 2006). The main difference is that earlier approaches are based on
495 Fourier descriptors or curvature profiling, but now we have a uniform description in a
496 Pythagorean-compact way (i.e. the structure of Equation 1 is the same as the Pythagorean
497 Theorem defining the circle; the Pythagorean Theorem results when, in Equation 1, $A=B=1$ and
498 the exponents $n_{1,2,3}=2$). In this way we can also encompass all different symmetries
499 encountered in diatoms, and provide for a quantitative measure for qualitative terms such as
500 elliptical or oval, (sub)circular and (sub-)spherical, crescent shapes, lanceolate, clavate,
501 naviculoid, sigmoid and more.

502 It should be noted that defining symmetry is still a major open problem in shape
503 description, and consequently in image analysis and automated detection. With Equations 1
504 and 2 however, no prior information is necessary since the system can itself determine the
505 symmetry of the shape (Gielis et al., 2011; Fougerolle et al., 2013). With the compact
506 description, associated characteristics such as surface area, volume, perimeter, curvature etc.
507 can be quantified immediately, and ratios can be used to understand optimal shapes and
508 distribution of pore. This leads to understanding of minimizing material use and optimization
509 of material distribution, mechanical strength and light focusing properties as discussed in
510 section 4. The very same principles apply in connected diatoms or in optimal packing of cells
511 in multicellular algae (Fig. 6). Given this uniform description, these characteristics are *a*
512 *priori*, whereas in existing systems where shapes are digitized, the characteristics need to be
513 computed *a posteriori*. Moreover, once geometrized, studies on mechanical stress can be
514 based on mesh free modeling, solving boundary value problems directly on the surfaces and
515 shells and complete frustrule. This allows for a global strategy for the geometric study of
516 diatoms, rather than based only on local properties.

517



518

Fig. 6. Left: Cell arrangement in *Zonaria turneriana*, Center: Antheridia of *Homoeostrichus sinclairii*, Right: Oogonium in *Homoeostrichus sinclairii*

519

520 3.2. Diatoms dealing with anisotropic stress

521 The proposed uniform description in diatoms can be very effective in the study of
 522 global properties, rather than local. Beyond shape description, we have to understand the
 523 forces that generate the shapes. The nearly universal principle in the natural sciences is that
 524 the equilibrium configuration of a system can be found by minimizing its total energy among
 525 all admissible configurations. When considering the surface as interface between two (or
 526 more) immiscible materials, the surface geometry is determined by minimizing the surface
 527 tension subject to whatever additional constraints are imposed by the environment. There is
 528 a canonical equilibrium surface, called the “Wulff shape”, that can be characterized as the
 529 absolute minimizer of the free energy F among all surfaces enclosing the same three-
 530 dimensional volume (Koiso and Palmer, 2008). Diatoms can be considered as Wulff shapes, on
 531 which surface stresses act, and they are the "unit spheres" for an anisotropic energy.

532 Surface stresses are determined geometrically by the curvatures of the surface (Gielis,
 533 2017). In surface theory it is well known that in each point of a surface one can find one
 534 maximum $\kappa_{max} = \kappa_1$ and one minimum curvature $\kappa_{min} = \kappa_2$ and the directions of these
 535 principal curvatures are always perpendicular. There are inevitable mathematical relations
 536 between these principal curvatures that fundamentally relate to the intrinsic nature of these

537 shapes (the Gaussian curvature $K = \kappa_1 \cdot \kappa_2$ or equivalently, is the square of the geometric
538 mean $GM = \sqrt{\kappa_1 \cdot \kappa_2}$ of the principal curvatures), or curvatures that fundamentally relate to
539 the shape, which these shapes assume in their ambient world, i.e. the extrinsic nature (given
540 by the mean curvature $H = \frac{\kappa_1 + \kappa_2}{2}$). Soap bubbles have constant mean curvature everywhere (
541 H is positive, not zero), but soap films (e.g. catenoids) are minimal surfaces with both K and H
542 equal zero, attaining equality $K = H^2 = 0$, in the inequality $K \leq H^2$.

543 Finding extremals of H^2 is another natural choice, embodied in the Willmore functional $\int H^2 dA$
544 (with dA area element) on closed surfaces in 3 dimensional space (Ferrandez, 2017). The
545 Willmore Theorem states that this functional is $\int H^2 dA \geq 4\pi$ with equality (and thus a
546 minimum) for the round sphere. The natural problem is to determine the minima when the
547 surfaces have additional constraints, topologically or metrically. This finds applications in
548 biology as the Helfrich energy for membranes (Ferrandez, 2017), relating to the cell
549 membrane of diatoms, which is the boundary between a living cell and its environment with
550 the frustule as the boundary shell, whose formation is guided by the silicalemma. With
551 Equations 1 and 2, we can study diatoms as Wulff shapes, minimizing certain anisotropic
552 energy functionals (Koiso and Palmer, 2008). The morphology of diatoms then can be studied
553 in the same way in which crystals, snowflakes, or soap films are studied. Many structures in
554 marine organisms are known to be periodic minimal surfaces, and the frustule structure of
555 diatoms is no exception. However, with the natural coordinate systems we can study
556 deviations from periodicity in real natural shapes.

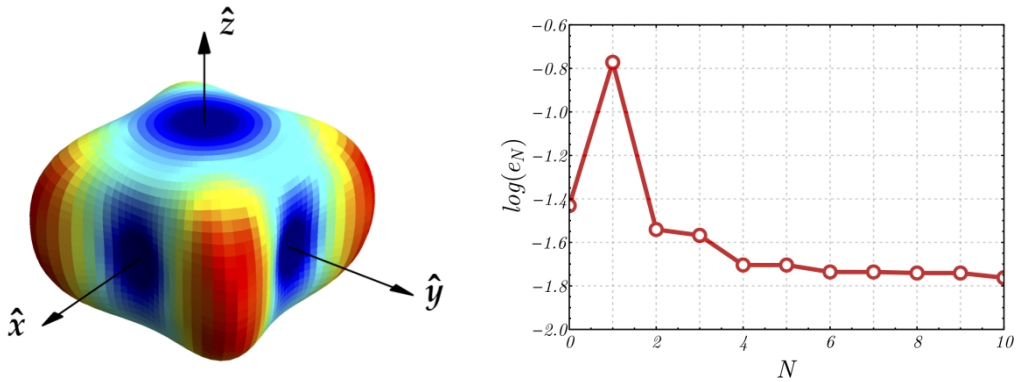
557

558 *3.3. Diatoms as biological model for mathematical physics and biomimicry*

559 Diatoms are a most natural domain for global and local studies of shape and
560 morphogenesis with geometry. Such shapes are striving for the status of ideal submanifold,
561 adapted to the surrounding space in a best possible way, in a dynamic equilibrium. The

562 surrounding space in this case contains large quantities of salt (silicic acid, NaOH etc.), typical
563 of generating specific shape variation. In very brine waters, archaeobacteria have been found
564 with triangular, square or box shapes (Bolhuis et al., 2006; Oren, 1999). The use of advanced
565 imaging techniques allows to determine both the global shape as well as the finest details of
566 the frustule, but from a mathematical point of view it is assumed that the frustule results as
567 the solution to boundary value problems by the organisms, within their environment. To
568 determine the associated boundary value problems and their solutions is the goal.

569 Fortunately, when the Gielis transformations were discovered, it was understood soon
570 that this could open the way for solving boundary value problems on any domain, using the
571 classical Fourier analysis. So far analytic Fourier-like solutions were restricted only to a few
572 domains, but can not be extended to a wide range of domains in 2D and 3D, without the need
573 for meshing and finite elements. Analytic Fourier-like solutions to Laplace, Helmholtz and
574 wave equations have been found for various 2D and 3D domains, including shells (Natalini et
575 al., 2008 and 2009; Caratelli et al., 2009; Caratelli et al., 2017). Fourier-like refers to analytic
576 solutions combining Fourier series, with special functions of Hankel and Bessel type. The
577 domains or shells are normal with respect to a suitable spherical coordinate system so that
578 the relevant boundary may be regarded as an anisotropically stretched unit circles or spheres.
579 The Laplacian is then defined for this anisotropically stretched coordinate system. In this
580 way, accurate solutions can be obtained with very low orders of expansions of spherical
581 harmonics. Fig. 7 shows one solution for the Robin problem for the Laplace equation on
582 closed shells with fourfold symmetry in the XY plane (Caratelli et al., 2017). This is generally
583 applicable for all 3D shells. These results show that, dependent on the boundary value
584 problem and the boundary conditions chosen, the solutions reflect the way shapes deal with
585 tensions on surfaces. In turn, these tensions are described by the mean curvature H , which is
586 directly related to the Laplacian Δ , due to a Theorem of Beltrami, namely $\Delta = 2H$ for surfaces.



588

589 **Fig. 7.** The solution of the Robin problem for the Laplace equation in a shell S with fourfold symmetry in XY
 590 direction. Left: Boundary behaviour along the inner shell surface of the partial sum U_N of order $N = 11$. Right: relative
 591 boundary error e_N as function of the order N of the truncated spherical harmonic expansion for the super-shaped shell on
 592 the left.

593

594 In Fig. 7, tensions are diverted to the corners in the shells, while top and bottom zones
 595 are essentially stress free. This solution is in line with the girdle of the frustule along one
 596 direction, while in the perpendicular direction (the lower and upper surface) the pores can
 597 form with their various functions. This is in line with the anisotropic mean curvature $\Lambda = \frac{T_1}{R_1} +$

598 $\frac{T_2}{R_2}$ (Koiso and Palmer, 2008; Thompson, 1917), the modification of the Laplace-Young formula,

599 wherein for given curvatures R_1 and R_2 , the tensions T_1 and T_2 in other directions determine a
 600 weighted arithmetic mean. This is observed in elongating plant cells, keeping the same width.

601 In dealing with stress, organisms can either avoid stress by aligning with the stress (e.g. wind

602 is converted into harmonics by trees) or by incorporating the stresses into form and function,

603 for example the floral shape on the test of sand dollars (Gielis, 2017). It is to be expected that

604 the shape of the upper and lower side of the frustule is the result of similar diverting of

605 stresses. In diverting and incorporating stresses, the shape of these upper and lower parts of

606 the frustule in centric diatoms for example may be considered as analogous to first modes of

607 vibration in drums. Likewise the precise shape and distribution of valves is the result of an

608 optimization problems.

609 These geometrical methods provide a more global view, which can be aligned in the
610 future with existing CAD and Finite Element studies in diatom frustules, but such global
611 geometric view is indispensable if we wish to understand form and function in diatoms. From
612 a geometrical point of view, diatoms are extremely interesting because the overall stable
613 geometrical structure of frustules, *costae* and other structures, is combined with local
614 optimization of the precise distribution of the pores. This distribution and the diversity make
615 diatoms individually unique; they are the snowflakes of (the liquid state of) water and they
616 are evolutionary very stable solutions.

617 The concept of stress imposed by the environment onto the boundary surface or shells,
618 has resulted in diatoms in structures capable of efficiently capturing light and radiation and of
619 dealing with specialized fluid and particle dynamics. In this sense diatoms have evolved as
620 excellent solutions, since the structure of the frustule gives the ability to focus light. This is a
621 concept also known in antenna, in particular in antenna arrays (Bia et al., 2017).
622 Understanding the structure of frustules can lead to new applications in technology
623 (biomimicry), but alternatively, concepts known only in technology, may be discovered in
624 living organisms as well. As one example, metamaterials are man-made materials with
625 negative index of refraction, not known in nature. However, metamaterials can easily be
626 obtained in various parts of the EM spectrum, by an array of supershapes (defined by
627 equation 1), to optimize or fine-tune spectral efficiency in antennas (Zhargooni et al., 2015) or
628 in light harvesting (Zhou et al., 2014).

629 It seems likely that the structure of the frustule provides the diatom with capabilities,
630 not only to focus light, but also to tune the reception of light in an optimal way. It aligns with
631 novel developments in antenna technology where electromagnetic bandgap structures are
632 used to create low loss dielectric structures based on periodicity of supershapes to prevent

633 propagation of certain frequencies, and increase isolation between antennas, and this can be
634 tailored on angle of incidence and polarization.

635 Also in fluid dynamics (see section 4) shapes defined by Equations 1 and 2 have been
636 used (Wang 2008; Legay and Zillian, 2008). Equations 1 and 2 have also been used in many
637 studies in nanotechnology (e.g. Tassadit et al., 2011; Macías et al., 2012; Forestiere et al.,
638 2015), in optimizing electro-osmotic pumps based on asymmetric silicon microchannel
639 membranes (Parashchenko et al., 2014) and in the study of dielectric properties of the skin
640 (Huclova et al., 2010).

641 This geometrical treatment of diatoms from a global viewpoint, should be integral part
642 of a systems biological approach, coupling insights on form and function to understand
643 genomic and genetic diversity in diatoms, during evolution and development. To solve the
644 boundary value problems they encounter, organisms can rely on a broad genetic toolbox and
645 set up to address problems through micro-RNAs, neofunctionalization, mobilisation of
646 transposable elements, epigenetic imprinting and so on. In diatoms this genetic toolbox is
647 known to be very complex with a rich history, and it is thus important to understand form and
648 function, since mathematical and physical laws are prevalent in our universe.

649

650 **4. PHYSICAL PROPERTIES OF THE FRUSTULE**

651

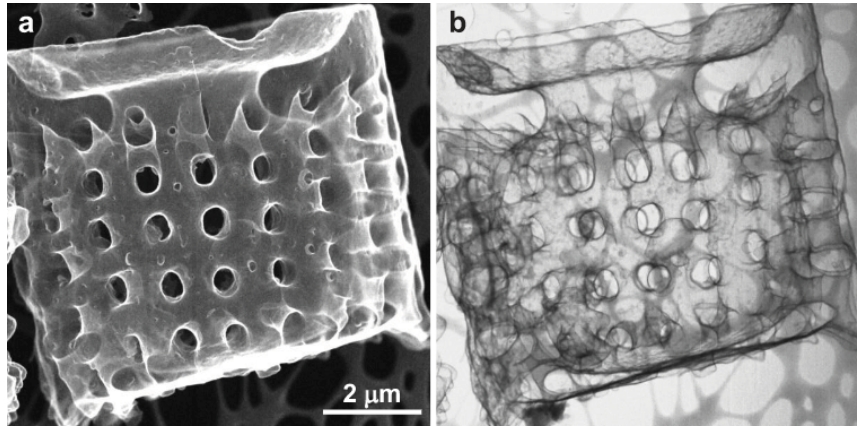
652 *4.1 Unveiling the frustule secrets*

653 While, in the first studies devoted to diatom biology, the main functionalities ascribed
654 to the frustule were related to protection of the cytoplasm from external, noxious agents and
655 to nutrient diffusion and uptake through its porous matrix, in the last decade new possible
656 evolutionary advantages have been hypothesized (Townley et al., 2011), including light
657 harvesting and focusing, carbon assimilation and sinking (Finkel et al., 2010).

658 Since the ultra-structured "anatomy" of the frustule, strictly related to its physical
659 properties and functionalities, is not visible in all its complexity by means of light microscopy,
660 it started to be revealed with the introduction, among other techniques, of transmission
661 electron microscopy (TEM), scanning electron microscopy (SEM), SEM stereo-imaging (Chen
662 et al., 2010) and atomic force microscopy (AFM) (Losic et al., 2007). In some cases two
663 different kinds of microscopy have been merged (photogrammetric surfaces derived from
664 SEM pictures plus confocal microscopy in Friedrichs et al., 2012 ; SEM plus digital holography
665 and SEM plus AFM in Ferrara et al., 2016), thus guaranteeing high levels of resolution and
666 accuracy in all three spatial dimensions. An accurate, precise and highly detailed
667 representation of frustule morphology is fundamental not only *per se*, but also in the retrieval
668 of CAD models for the numerical simulation and systematic study of its physical properties,
669 mainly mechanical, fluid-dynamical and optical.

670 A recent technique introduced by Pan et al. (Pan et al., 2014), allowed the detailed
671 investigation of the internal structure of diatom frustules without sectioning the silica walls of
672 the shell. Indeed they obtained graphene replicas of *Aulacoseira* genus frustules by means of
673 chemical vapor deposition of methane. Since graphene is highly transparent to electron
674 beams, this allows the visualization of the internal morphology and structure of valves and
675 girdles, unveiling the intricate, interconnected nanotubes linking their different layers (see
676 Fig. 8). This is of fundamental importance in the understanding of the interactions of the living
677 cell with the external environment and relative exchanges of matter.

678



679

680 **Fig. 8.** SEM mode (a) and TEM mode (b) STEM images of a graphene replica of a single *Alaucoseira* frustule.

681 Courtesy of Pan et al., 2014.

682

683 *4.2 Mechanical properties of the frustule*

684 The study of the mechanical properties of frustules is of great interest not only in the
685 understanding of their functionalities, but also in the framework of biomimetics applied to
686 nanotechnology (Gordon et al., 2009), architecture (Bach et al., 1985), and lightweight
687 constructions (Hamm et al., 2005).

688 In 2003, Hamm and coworkers (Hamm et al., 2003) experimentally measured and
689 numerically simulated the forces necessary to break the frustules of three species of diatoms:
690 *Thalassiosira punctigera* (centric), *Coscinodiscus granii* (centric and much larger than *T.*
691 *punctigera*) and *Fragilariopsis kerguelensis* (pennate). Using calibrated glass microneedles to
692 load and break the frustules with defined forces, they found that they were able to resist to
693 pressures ranging from 1 to 7 N/mm², equivalent to 100-700 tonnes/m². Measurements on an
694 isolated pleura (i.e. an open, hoop-shaped segment of the girdle) of *T. punctigera* allowed to
695 estimate its Young's modulus E in about 22.4 GPa, comparable to those of cortical bone or
696 medical dental composites.

697 One way to understand how stresses are distributed through the ultrastructure of a
698 frustule after mechanical solicitation is to make use of the Finite Element Method (FEM). In
699 this kind of analysis, the object under study is discretized into a finite number of parts (the

700 elements, indeed), which is equivalent to say that the domain is reduced into a limited
701 number of degrees of freedom. Once a complete set of elements (the so called *mesh*) is
702 obtained, the response of the system to applied forces is described by a system of partial
703 differential equations acting at the interconnected joints between the elements (the so called
704 *nodes*) which cannot be solved analytically. We can bypass this difficulty assuming that, in
705 each element, the response to the solicitation is predefined (e.g. linear in case of mechanical
706 forces). Even though FEM can readily handle complex geometries and a wide variety of
707 physical problems (mechanical, thermodynamical, fluid-dynamical and electrostatic
708 problems), we have to keep in mind that it is able to produce only approximate, not closed-
709 form solutions (see section 3). In the next generation studies of diatoms, these methods can
710 be combined with the geometrical model of section 3, which allow for analytic solutions and
711 global geometry.

712 Looking at finite element model (FEM) numerical simulations performed on a rendered,
713 complete frustule of *F. kerguelensis*, Hamm et al. concluded that the presence of ribs (the so
714 called *costae*) allowed to deflect stress concentration, smoothly absorbing it from the fragile
715 areas in between.

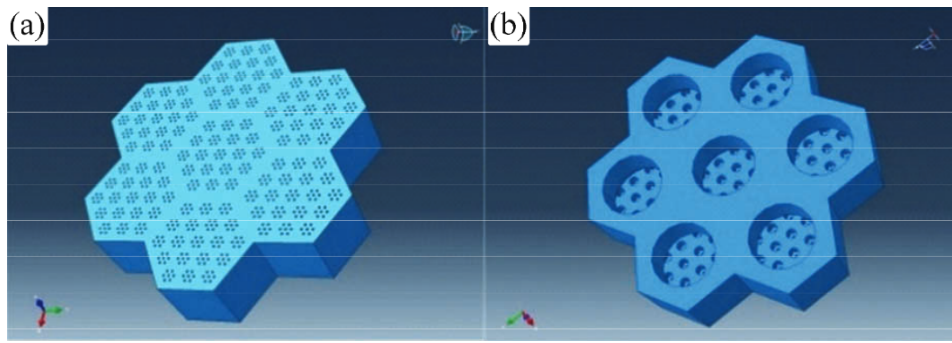
716 Moreno et al. (Moreno et al., 2015) tried to quantify even more in detail the different
717 response to mechanical stress of centric (*Coscinodiscus* sp.) and pennate (*Synedra* sp.) diatom
718 frustules. By means of nanoindentation measurements they derived, for *Coscinodiscus* sp.
719 frustules, values of E ranging in the interval 1.1-10.6 GPa and a hardness module H of 0.10-
720 1.03 GPa, respectively. The analogous values for *Synedra* sp. varied between 13.7 and 18.6
721 GPa and 0.85 and 1.41 GPa, respectively. Successive FEM simulations on accurate CAD models
722 allowed to shed light on this different response to mechanical stimuli. The higher robustness
723 of *Synedra* sp. frustules is mostly due to their high aspect ratio and rib-slit structure. On the
724 other hand, stress levels in *Coscinodiscus* sp. are strongly dependent on pore dimension:

725 increasing pore size leads to an improved and more flexible structure.

726 Recently, the combination of nanoindentation and three-point bending tests allowed to
727 retrieve even more accurately the elastic modulus of valves and girdles of *Coscinodiscus* sp.
728 frustules, obtaining an average value of 36 ± 8 GPa (Aitken et al., 2016): it follows that the
729 diatom frustule is characterized by a specific strength much larger than any other reported
730 natural biomaterial, mainly due to the honeycomb multi-layer architecture of the valves.

731 In general, numerical simulations are unavoidable if the complex relationship between
732 mechanical properties of the frustule and its detailed features (porosity, shape, thickness,
733 pore size etc.) has to be analyzed. Lu et al. (Lu et al., 2015) modeled with high accuracy the
734 valve of a *Coscinodiscus* sp. diatom starting from a unit cell which comprised all the three
735 layers of the valve (*foramen*, *cribrum* and *cribellum*) and even taking into account the
736 curvature of the walls of foramen pores (*areolae* chambers). The actual lattice which repeats
737 periodically throughout the valve is constituted by seven of these unit cells arranged with
738 hexagonal symmetry (see Fig. 9). This model has been compared with a reference, solid
739 structure with no pores at all but with the same amount of material. FEM simulations allowed
740 to conclude that, in presence of pores, the seven-unit-cell (and the corresponding larger scale
741 structure obtained by expanding it in two dimensions) is able to lower the stress
742 concentration at the edges (in elastic regime) with respect to the solid reference; the average
743 stress level and edge stress concentration are lower than those in the reference structure; the
744 stress is lower between the pores. Hence, in a diatom frustule, material is saved while a
745 certain level of strength is maintained (this allows to explain the elevated silica circle around
746 the pores of the foramen, which allows to strengthen the structure locally). Analogous
747 simulations performed on a simplified model of the girdle led to the conclusion that a larger
748 reaction force is observed compared to the reference structure, which indicates that the girdle
749 band can withstand larger compression forces (see again Hamm et al., 2003).

750



751

752 **Fig. 9.** Outer (a) and inner (b) view of the seven-unit cell used in Lu et al. (2015) to simulate the response of
753 *Coscinodiscus* sp. valves to mechanical stimuli. Reproduced with permission.

754

755 Even though many organisms, from protists to crustacean zooplankton, feed on diatoms,
756 the hypothesis that one of the main functionalities of diatom frustules is protection and
757 defense from predators is not to be excluded. Indeed, any mechanism able to reduce
758 population mortality in an environment strongly dominated by grazing pressure is
759 advantageous. Furthermore, diatoms can survive gut passage if frustules are not crushed and
760 it is likely that silica-edged mandibles of copepods and euphausiids co-evolved with their
761 diatom preys (Hamm et al., 2003). The intimate relationship between the silification process
762 and grazing pressure has been deeply studied by Pondaven and coworkers (Pondaven et al.,
763 2007). As we mentioned in section 2, it was already known that, under iron, nitrogen,
764 phosphorous or light limitations a decrease in diatom growth rate and an increase in frustule
765 silica content take place (Brzezinski, 1985). What has been observed further is that grazing
766 pressure induces variations in cell wall silification of the same order of magnitude as those
767 determined by changes in growth environment, with consequent, significant variations in
768 Si:N and Si:C ratios. This behavior could, to some extent, allow to understand the variability in
769 the grade of silification that can be found from species to species according to their specific
770 environment.

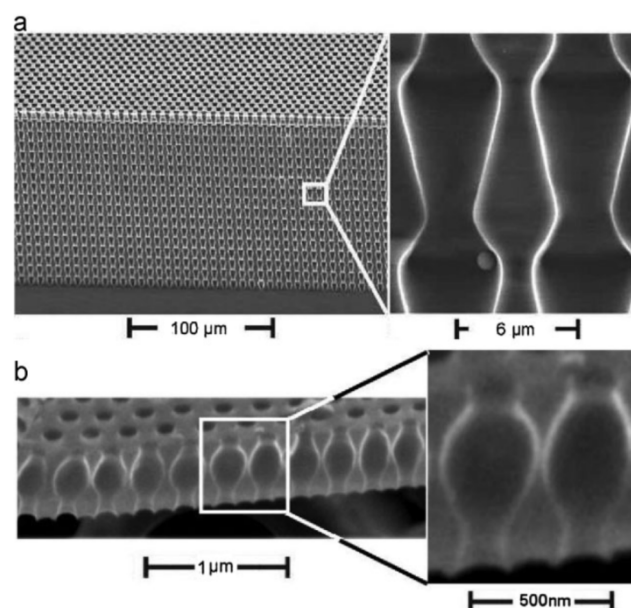
771

772 4.3 Diatom frustule fluid dynamics

773 One of the main functionalities that has been ascribed to diatom frustules is the capability
774 to sort and filter nutrients (such as NH_4^+ , HCO_3^- , NO_3^- etc.) from harmful agents (e.g. bacteria
775 and viruses). The involved concentrations range from $\sim 10^6 \text{ ml}^{-1}$ for bacteria (0.2-1 μm in
776 dimension), $\sim 10^7 \text{ ml}^{-1}$ for viruses (20-200 nm) up to $\sim 10^9 \text{ ml}^{-1}$ for colloids (5 nm-2 μm) and
777 $\sim 10^{14} \text{ ml}^{-1}$ for nutrient molecules.

778 The first interaction of these living and non-living brownian particles with diatoms is, of
779 course, with the external surface of frustules. Hale and coworkers (Hale et al., 2001; Hale et
780 al., 2002) showed experimentally, for *Coscinodiscus* sp. and *Thalassiosira eccentrica* diatoms,
781 that both diffusion and advection of sub-micrometric beads are altered by the micro-
782 topographies of the frustule. In particular, beads following streamlines in a fluid in proximity
783 of the frustule are directed around the edges of the areolae localizing themselves in proximity
784 of areolae ridges, thus deflecting from the direction of bulk flow. Since the magnitude of this
785 effect is strictly dependent on the ratio a/R_0 of the bead and areola radii, it could constitute an
786 elegant way to sort particles according to their size. Furthermore, looking at the transverse
787 section of a *Coscinodiscus* sp girdle, it can be noticed how the profile of the pore channels
788 presents impressive similarity with that of a typical silicon drift ratchet (Losic et al., 2009; see
789 Fig. 9). A drift ratchet membrane is provided with microchannels made of a periodic series of
790 ratchet-shaped pores (i.e. with a periodic but asymmetric variation of the diameter along the
791 pore axis), which, in zero-mean fluid flow conditions, generates a rectified motion in finite-
792 sized brownian particles. This means that, even though the mean value of the periodic
793 pressure profile is zero, a net motion of particles suspended in the fluid from one side of the
794 membrane to the other can be observed, with no motion of the liquid itself (Matthias et al.,
795 2003). In a drift ratchet, the direction of the particle current depends very sensitively on the
796 size of the particles, even though this effect is difficult to predict intuitively (Kettner et al.,

797 2000). This could represent a further contribute to particle sorting according to size.
798 Nevertheless, the main differences between an artificial drift ratchet and the section of a
799 *Coscinodiscus* sp girdle are quite relevant. The girdle band pores have only two repeating
800 units in series respect to the tens of units of an artificial drift ratchet (Fig. 10a), so we are
801 definitively far from the assumption of an idealized infinitely long and exactly periodic
802 channel, on which the stochastic models relating the direction of motion of the particles and
803 particle size are based; the girdle pores are subjected to different and more variable fluid
804 oscillations in the oceanic environment; finally, the dimensions of the pores are of the order of
805 the fractions of micrometer versus the several micrometers of a typical artificial drift ratchet
806 silicon membrane. However, the fabrication of biomimetic, diatom-inspired silica ratchets
807 would shed light on the possible ability of frustule girdles to induce asymmetric diffusion on
808 particles dispersed in an aquatic environment.



809
810 **Fig. 10.** Artificial silicon ratchet membrane (a) and cross-section of a *Coscinodiscus* sp. diatom girdle (b). Courtesy of
811 Losic et al., 2009.

812
813 Even the formation of colonies in the shape of chains, which characterizes several species
814 of diatoms (Round et al., 1990), and their fluid dynamic interaction with the environment,

815 seems to have some influence on the efficiency of nutrients uptake. Srajer et al. (Srajer et al.,
816 2009) applied simulations based on Computational Fluid Dynamics (CFD) on a simplified
817 model describing a colony comprised of single units of 10 cells repeated endlessly. It turns out
818 that the interaction of the chain with unsteady flow conditions triggers oscillatory variations
819 in the distance between adjacent cells, increasing advective diffusion through the surface of
820 the diatoms and therefore nutrient supply. However, this simplified model does not take into
821 account the presence of linking spines or periplekton between adjacent cells. Since, actually,
822 the spaces between single diatoms of a chain contain linking elements, viscosity will tend to
823 suppress inter-cell flows. Nevertheless, the gaps still contribute to reduction of the biomass
824 per unit chain length, thus increasing the nutrient supply for each cell (Pahlow et al., 1997).

825 Another fundamental phenomenon involving frustule fluid dynamics is certainly sinking
826 rate (Miklasz et al., 2010)]. Being the main photosynthesizers of the ocean and generating half
827 of its fixed carbon every year (Field et al., 1998), the maximum speed at which diatoms sink
828 strongly influences global carbon cycle besides silicon fluxes. The accurate prediction of
829 maximum sinking speed could thus allow to calculate carbon and silicon oceanic fluxes
830 starting from local measurement of production (Nelson et al., 1995).

831 Usually, the sinking rate U of a spherical particle immersed in a fluid is dependent by the
832 radius r and density ρ of the particle, the density ρ_f of the fluid and its dynamic viscosity μ ,
833 according to the well known Stokes' law:

834

$$835 \quad U = \frac{2(\rho - \rho_f)gr^2}{9\mu}$$

836

837 where g is the gravitational acceleration.

838 Diatoms are able to reduce their density through ion exchange (Anderson et al., 1978;

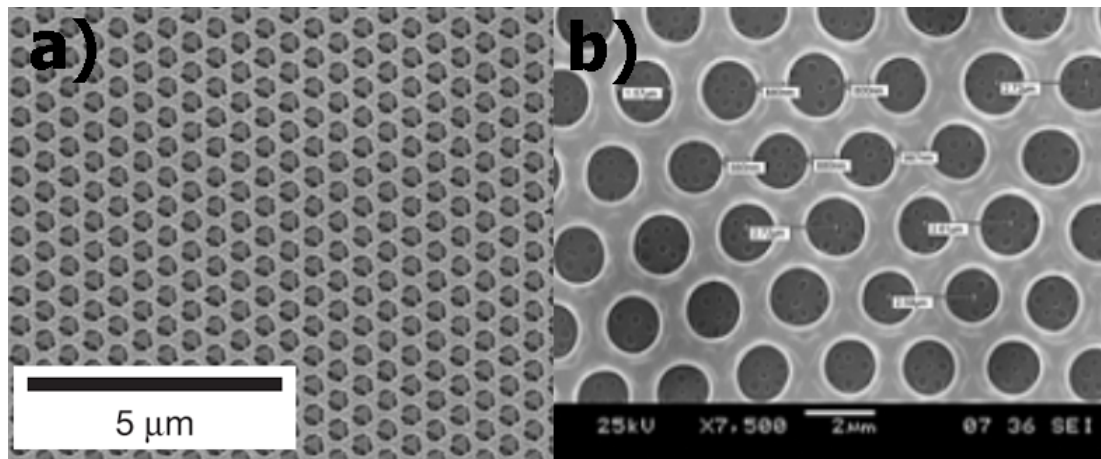
839 Waite et al., 1997), but in the absence of physiological density reduction, they sink at their
840 maximum speed. According to Stokes' law, the sinking velocity of a spherical particle scales
841 with the radius squared, which is not true for a diatom (both live or dead), since its
842 approximation to a sphere is quite inaccurate. Miklasz et al. (Miklasz et al., 2010) corrected
843 Stokes' law taking into account the relative contribution of frustule and cytoplasm densities,
844 the geometry of the frustule and its thickness, thus obtaining predictions that fit more
845 accurately with experimental data. Indeed, typically diatom sinking rate depends on diatom
846 radius with a scaling exponent between 1.2 and 1.6 (Smayda et al., 1970; Waite et al., 1997).
847 Thus it is straightforward to deduce that, lowering the sinking speed, the peculiar shape and
848 morphology of the frustule allows for a longer stay of diatoms near ocean surface and,
849 consequently, a longer exposition to sunlight than if they were provided with a simple,
850 spherical porous silica armor.

851

852 *4.4 Optical properties of the frustule*

853 The impressive similarity of diatom frustules with artificial photonic crystals (Fuhrmann
854 et al., 2004; De Stefano et al., 2009) (Fig. 11) induced to hypothesize that, beyond mechanical
855 defense and filtering of nutrients from harmful agents, valves and girdles could play a
856 fundamental role in light manipulation and harvesting, thus enhancing photosynthetic
857 efficiency in environments where light is not so easily accessible.

858



859

860 **Fig. 11.** Artificial photonic crystal (a) and detail of a single valve of *Coscinodiscus wailesii* diatom (b). (a) is
 861 reproduced with permission from Qi et al., 2004; (b) is reproduced with permission from De Stefano et al., 2007.

862

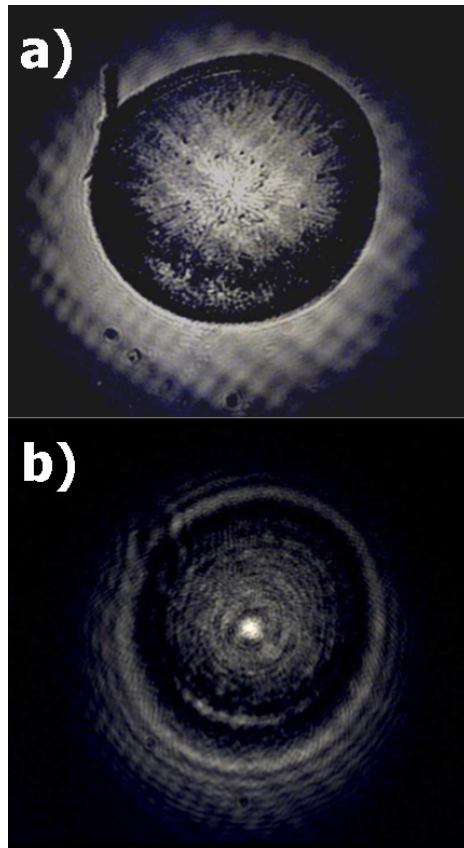
863 A photonic crystal is constituted by a spatial, periodic distribution of refractive index
 864 which, properly dimensioned, can block the propagation of light in specific wavelength ranges
 865 (the so-called *photonic band-gaps*) (Joannopoulos et al., 2008). Several animals and plants,
 866 mainly insects, birds and flowers, developed, through billions of years of evolution and as
 867 constitutive part of their organisms, sub-micron, periodic or quasi-periodic architectures
 868 which substantially act as photonic crystals, giving rise, by means of selective transmittance
 869 and reflectance at different wavelengths, to so-called structural colors (Vukusic et al., 2003;
 870 Parker et al., 2007; Kolle, 2011; Greanya, 2016). Structural colors are not due to any pigment
 871 but only to the geometrical characteristics and refractive index of micro- and nanostructured
 872 scales, cuticles, plumage and similar features.

873 The interaction of diatom frustules with light is even more articulate, and consists of
 874 three main phenomena: light confinement, selective transmission and photoluminescence.

875 In 2007 De Luca et al. (De Stefano et al., 2007) first observed light confinement by a single
 876 valve of *C. wailesii*, about 150 μm in diameter. The experiment was conducted with red
 877 coherent radiation, and the incoming beam was focused by the valve in a tiny spot < 10 μm
 878 wide at a distance of about 100 μm from it (Fig. 12). Even though, from this point of view, *C.*

879 *wallesii* valves can be assimilated to a sort of microlenses, the phenomenon is to be ascribed
880 to diffraction rather than refraction: numerical simulations (De Tommasi et al., 2010; Ferrara
881 et al., 2014) confirmed indeed that light confinement is due to the coherent superposition of
882 the diffraction contributions coming from the single pores. The same effect can be observed
883 making use of digital holography (DH) (Di Caprio et al., 2014; Ferrara et al., 2014), which
884 allows to retrieve both intensity and phase of the radiation transmitted by the valve. After the
885 acquisition of the hologram of a single diatom valve in a typical Mach-Zender interferometer
886 and the application of a proper algorithm (described in detail in Di Caprio et al., 2014), the
887 intensity and phase of the optical field interacting with it can be retrieved at every point of the
888 direction of propagation of the laser beam. Among the advantages of this method, there is the
889 possibility to analyze light propagation in a medium different than air, just substituting the
890 proper refractive index in the reconstruction algorithm. Both DH measurements and previous
891 numerical simulations based on Wide Angle Beam Propagation Method (De Tommasi et al.,
892 2010; Ferrara et al., 2014) demonstrated that, in water and in cytoplasm, the confinement of
893 incoming light takes place closer to the valve if compared to air, thus increasing light
894 collection inside the cell.

895



896

897 **Fig. 12.** “Focusing effect” by a single valve of *Coscinodiscus wailesii* diatom. Image acquired at 4 (a) and 104 (b)
898 microns from the valve Courtesy of De Stefano et al., 2007.

899

900 The diffractive character of the effect was scrutinized by Noyes et al. (Noyes et al., 2008).
901 An Euler cradle (traditionally applied in X-ray diffraction characterization of crystals),
902 allowed to analyze intensity and orientation of light transmitted by single valves of *C. wailesii*
903 diatoms, after irradiation with blue (472 nm), green (543 nm) and red (633 nm) laser light.
904 Red light transmission was more efficient than blue and green ones, by a factor of 3.5 and 2.5
905 respectively. Light which is not transmitted, reflected or scattered by the valve, is supposed to
906 couple to girdle and valves (acting as sort of waveguides) as already experimentally
907 demonstrated by Fuhrmann et al. (Fuhrmann et al., 2004). It is noteworthy that, in the
908 spectral range between 630 and 675 nm, we can find a peak in the absorption spectrum of
909 chlorophyll *a*, one of the main molecules involved in photosynthesis (Kirk, 2011). Since
910 diatoms interact with sunlight and not with laser radiation, a lot of work has been performed

911 in recent years and by several authors (De Tommasi et al., 2010; Hsu et al., 2012; Ferrara et
912 al., 2014; Romann et al., 2015) making use of incoherent sources of illumination. The obtained
913 results confirm the presence of the same focusing effect, which is characterized by a precise
914 and reproducible behavior as a function of the incoming wavelength, also confirmed by
915 numerical simulations. The longer the wavelength, indeed, the closer to the valve the "focal
916 spot" takes place, which is easily understandable if we look at the dependence of diffraction
917 angle from a circular aperture (in this case the single pore of the valve) by the wavelength of
918 the incoming radiation (Born and Wolf, 1993). This implies that, for sufficiently short
919 wavelengths, the superposition of diffractive contributions takes place far beyond the frustule
920 or it does not takes place at all. In case of *Arachnoidiscus* sp diatoms, for example, UVB
921 transmitted radiation reaches, in air, the first intensity peak at about 500 μm from the valve,
922 while, on the opposite, for red light we have a first maximum at about 90 μm from the valve
923 and an intensity enhancement of more than three times respect to incident radiation (Ferrara
924 et al., 2014). This behavior is one of the mechanisms by which diatom frustules are able to
925 screen the cell from harmful UV radiation, the other being absorption by the amorphous,
926 hydrated silica of the frustule itself. Actually still another photonic property of diatom
927 frustules results in efficient conversion of harmful UV radiation into photosynthetically active
928 radiation (PAR). Indeed, since diatom frustules are made by nanostructured silica full of
929 surface defects and incorporated organic compounds, they are characterized by intense
930 photoluminescence if irradiated at the proper wavelength (Qin et al., 2008). In particular, they
931 emit blue radiation if irradiated with UVB light, which means that noxious radiation able to
932 promote the formation of pyrimidine dimers in DNA strands is converted into radiation
933 spectrally located in correspondence of one of the maxima of photosynthesis action spectrum
934 (De Tommasi, 2016). Indeed, around 450 nm fucoxanthine (which is one of the main pigments
935 found in diatom chloroplasts) has a significant absorption band.

936 The ability of centric diatom frustules to couple efficiently to visible radiation and confine
937 it in local "hot spots" may be strictly related to chloroplast mobility as a function of
938 illumination conditions. It is known indeed that, under dim light conditions, chloroplasts of
939 centric diatoms tend to locate close to frustule walls (Furukawa et al., 1998), where light is
940 guided by valves and girdles (as observed in Fuhrmann et al., 2004). On the other side, under
941 intense illumination, chloroplasts migrate towards the centre of the cell, where light
942 confinement has its maximum, this migration being pronounced for blue irradiation (Shihira-
943 Ishikawa et al., 2007). This could represent a double advantage, since it would allow both to
944 protect the nucleus from photodamage and simultaneously collect with high efficiency
945 radiation which fits the absorption spectra of chlorophylls.

946

947

948

949

950 **5. CONCLUSIONS**

951

952 Many questions concerning diatom frustule morphogenesis remain unresolved, and only
953 an integrated, multidisciplinary approach, spanning from genetics to geometry and physics,
954 would represent an effective instrument in the understanding of the complex relationships
955 which link frustule formation, shape diversity, and functionalities. Species-specific shapes,
956 dimensions and pore patterns indicate a strict genetic control on frustule morphogenesis and
957 functional analyses of the related proteins are necessary. Such analyses require the ability to
958 generate overexpressing strains and knockout cell wall mutants. The potential applications of
959 such tools in basic diatoms biology research, as well as in applied research are huge. However,
960 all the contributions are complementary: the characterization of biosilica synthesis and the

961 possibility to modulate the expression of the genes encoding for the frustule-associated
962 proteins will provide unique samples for optical, photonic, microfluidic and mechanical
963 analysis in order to understand which shape optimize better light collection, nutrient uptake
964 and mechanical resistance. In this context, shape is the fundamental link between frustule
965 morphogenesis and its functionalities. Finding the more suitable mathematical tool to
966 generate, describe and understand shapes under specific environmental and functional
967 constraints will give an extraordinary contribution in unveiling diatom diversity and
968 dominance as major photosynthetic group in oceans.

969

970 **COMPETING INTERESTS**

971 The authors declare that there is no conflict of interests regarding the publication of this
972 paper.

973

974 **ACKNOWLEDGMENTS**

975 The authors are grateful to Albert Kiefer, visual designer, for producing the scientific images,
976 to Prof. Carla Langella and Dr. Antonia Auletta from the Department of Architecture and
977 Industrial Design of the University of Campania “Luigi Vanvitelli” for the realization of the 3D
978 CAD models of centric diatom frustules and to Dr. Angela Falciatore from the Institut de
979 Biologie Paris-Seine of the Sorbonne Universités, CNRS-UPMC, Paris and Dr. Carlo Fasano for
980 their critical suggestions to improve the manuscript.

981

982

983

984

985
986
987
988
989
990
991
992
993
994
995
996
997
998

999 **REFERENCES**

1000

1001 Aitken, Z. H., Luo, S., Reynolds, S. N., Thaulow, C., and Greer, J. R., 2016. Microstructure
1002 provides insights into evolutionary design and resilience of *Coscinodiscus* sp. frustule. Proc.
1003 Natl. Acad. Sci. USA. 113: 2017-2011.

1004 Allen, A. E., LaRoche, J., Maheswari, U., et al., 2008. Whole-cell response of the pennate diatom
1005 *Phaeodactylum tricornutum* to iron starvation. Proc. Natl. Acad. Sci. USA., 105: 10438–10443.

1006

1007 Anderson, L. W. J., Sweeney, B. M., 1978. Role of inorganic ions in controlling sedimentation
1008 rate of a marine centric diatom *Ditylum brightwelli*. J. Phycol. 14: 204-214.

1009 Antonelli, P. L., & Miron, R. (Eds.), 2013. *Lagrange and Finsler Geometry: Applications to*

1010 *Physics and Biology* (Vol. 76). Springer Science & Business Media.

1011

1012 Apt, K.E., Kroth-Pancic, P.G., Grossman, A.R., 1996. Stable nuclear transformation of the diatom
1013 *Phaeodactylum tricornutum*. *Mol. Gen. Genet.* 252, 572–579. A

1014

1015 Armbrust, E.V., Berges, J.A., Bowler, C., Green, B.R., Martinez, D., Putnam, N.H., Zhou, S., Allen,
1016 A.E., Apt, K.E., Bechner, M., Brzezinski, M.A., Chaal, B.K., Chiovitti, A., Davis, A.K., Demarest,
1017 M.S., Detter, J.C., Glavina, T., Goodstein, D., Hadi, M.Z., Hellsten, U., Hildebrand, M., Jenkins, B.D.,
1018 Jurka, J., Kapitonov, V.V., Kroger, N., Lau, W.W., Lane, T.W., Larimer, F.W., Lippmeier, J.C.,
1019 Lucas, S., Medina, M., Montsant, A., Obornik, M., Parker, M.S., Palenik, B., Pazour, G.J.,
1020 Richardson, P.M., Rynearson, T.A., Saito, M.A., Schwartz, D.C., Thamtrakoln, K., Valentin, K.,
1021 Vardi, A., Wilkerson, F.P., Rokhsar, D.S., 2004. The genome of the diatom *Thalassiosira*
1022 *pseudonana*: ecology, evolution, and metabolism. *Science* 306, 79–86.

1023

1024 Arnold, V. I., 1998. On teaching mathematics. Extended text of the address for the discussion
1025 on teaching of mathematics in Palais de Découverte in Paris on 7 March 1997

1026

1027 Bach, K., 1985. IL 28 Diatoms 1: Shells in Nature and Techniques. Karl Kramer Verlag,
1028 Stuttgart.

1029 Bao, Z., Weatherspoon, M. R., Shian, S., Cai, Y., Graham, P. D., Allan, S. M., Ahmad, G., Dickerson,
1030 M. B., Church, B. C., Kang, Z., Abernathy III, H. W., Summers, C. J., Liu, M., Sandhage, K. H., 2007.
1031 Chemical reduction of three-dimensional silica micro-assemblies into microporous silicon
1032 replicas. *Nature* 446, 172-175.

1033

1034 Basu, S., Patil, S., Mapleson, D., Russo, M.T., Vitale, L., Fevola, C., Maumus, F., Casotti, R., Mock,
1035 T., Caccamo, M., Montresor, M., Sanges, R., Ferrante, M.I., 2017. Finding a partner in the ocean:
1036 molecular and evolutionary bases of the response to sexual cues in a planktonic diatom. *New*
1037 *Phytol.* 215(1):140-156.

1038 Berger, M., 2003. A panoramic view of Riemannian geometry. Springer Verlag.
1039 doi:10.1007/978-3-642-18245-7

1040

1041 Bia, P., Caratelli, D., Mescia, L., Gielis, J., 2015. Analysis and synthesis of supershaped dielectric
1042 lens antennas. *IET MICROWAVES ANTENNAS PROPAG.*, 9(14), 1497-1504.

1043

1044 Bogaert, K. A., Beeckman, T., & De Clerck, O., 2017. Two-step cell polarization in algal zygotes.
1045 *Nat. Plants* 3, 16221.

1046

1047 Bolhuis, H., Palm, P., Wende, A., Falb, M., Rampp, M., Rodriguez-Valera, F., et al., Oesterhelt, D.
1048 2006. The genome of the square archaeon *Haloquadratum walsbyi*: life at the limits of water
1049 activity. *BMC Genomics* 7(1), 169.

1050

1051 Born, M., Wolf, E., 1993. Principle of Optics 6th edition, Pergamon Press, Oxford.

1052 Brzezinski, M. A., 1985. The Si:C:N ratio of marine diatoms: interspecific variability and the
1053 effect of some environmental variables. *J. Phycol.* 21, 347-357.

1054

1055 Brzezinski, M. A., 2008. Mining the diatom genome for the mechanism of biosilicification. *Proc.*
1056 *Natl. Acad. Sci. U S A.* 5; 105(5): 1391–1392.

1057 Bridoux, M. C., Ingalls, A. E., 2010. Structural identification of long-chain polyamines

1058 associated with diatom biosilica in a Southern Ocean sediment core. *Geochim. Cosmochim.*
1059 *Acta* 74; 14, 15 4044–4057.

1060

1061 Bowler, C., Allen, A.E., Badger, J.H., Grimwood, J., Jabbari, K., Kuo, A., Maheswari, U., Martens, C.,
1062 Maumus, F., Otilar, R.P., Rayko, E., Salamov, A., Vandepoele, K., Beszteri, B., Gruber, A., Heijde,
1063 M., Katinka, M., Mock, T., Valentin, K., Verret, F., Berges, J.A., Brownlee, C., Cadoret, J.P.,
1064 Chiovitti, A., Choi, C.J., Coesel, S., De Martino, A., Detter, J.C., Durkin, C., Falciatore, A., Fournet,
1065 J., Haruta, M., Huysman, M.J., Jenkins, B.D., Jiroutova, K., Jorgensen, R.E., Joubert, Y., Kaplan, A.,
1066 Kroger, N., Kroth, P.G., La Roche, J., Lindquist, E., Lommer, M., Martin-Jezequel, V., Lopez, P.J.,
1067 Lucas, S., Mangogna, M., McGinnis, K., Medlin, L.K., Montsant, A., Oudot-Le Secq, M.P., Napoli, C.,
1068 Obornik, M., Parker, M.S., Petit, J.L., Porcel, B.M., Poulsen, N., Robison, M., Rychlewski, L.,
1069 Rynearson, T.A., Schmutz, J., Shapiro, H., Siaut, M., Stanley, M., Sussman, M.R., Taylor, A.R.,
1070 Vardi, A., von Dassow, P., Vyverman, W., Willis, A., Wyrwicz, L.S., Rokhsar, D.S., Weissenbach, J.,
1071 Armbrust, E.V., Green, B.R., Van de Peer, Y., Grigoriev, I.V., 2008. The *Phaeodactylum* genome
1072 reveals the evolutionary history of diatom genomes. *Nature* 456, 239–244.

1073

1074 Bhattacharya P., Volcani B. E., 1980. Sodium-dependent silicate transport in the apochlorotic
1075 marine diatom *Nitzschia alba*. *Proc. Natl Acad. Sci. USA* 77, 6386–6390.

1076

1077 Brunner E., et al., 2009. Chitin-based organic networks: An integral part of cell wall biosilica in
1078 the diatom *Thalassiosira pseudonana*. *Angew. Chem. Int. Ed* 48:9724–9727.

1079

1080 Bucciarelli, E., Pondaven, P., Sarthou, G., 2010. Effects of an iron-light co-limitation on the
1081 elemental composition (Si, C, N) of the diatoms *Thalassiosira oceanica* and *Ditylum*
1082 *brightwellii*. *Biogeosci.* 7: 657–669.

1083

1084 Caratelli, et al., 2009. Fourier solution of the Dirichlet problem for the Laplace and Helmholtz
1085 equations in starlike domains. Lecture Notes of TICMI, 10.

1086

1087 Caratelli, D., Natalini, P., Ricci, P.E., 2017. Spherical Harmonic Solution of the Robin Problem
1088 for the Laplace Equation in Supershaped Shells. Atlantis Transactions in Geom, Vol 2, 17-30.
1089 Atlantis-Springer.

1090

1091 Chen, X., Ostadi, H., Jiang, K., 2010. Three-dimensional surface reconstruction of diatomaceous
1092 frustules. Anal. Biochem. 403: 63-66.

1093

1094 Claquin, P., Martin-Jézéquel, V., Kromkamp, J. C., Veldhuis, M. J. W., Kraay, G. W., 2002.
1095 Uncoupling of silicon compared with carbon and nitrogen metabolism and the role of the cell
1096 cycle in continuous cultures of *Thalassiosira pseudonana* (Bacillariophyceae) under light,
1097 nitrogen, and phosphorus control. J. Phycol. 38: 922–930.

1098

1099

1100 Daboussi, F., Leduc, S., A. M., Dubois, G., Guyot, V., Perez-Michaut, C., Amato, A., Falciatore, A.,
1101 Juillerat, A., Beurdeley, M., Voytas, D.F., Cavarec, L., Duchateau, P., 2014. Genome engineering
1102 empowers the diatom *Phaeodactylum tricornutum* for biotechnology. Nat. Commun. 5, 3831.

1103

1104 Dhar, Pawan K., and Alessandro, G., 2010. Laws of Biology: Why so Few? *Systems and*
1105 *Synthetic Biology* 4.1 (2010): 7–13. *PMC*. Web. 21 Mar. 2017.

1106

1107 Darwin, C. 1859. On the Origin of Species by Means of Natural Selection. J. Murray, London

1108

1109 Delalat, B., Sheppard, V. C., Rasi Ghaemi, S., Rao, S., Prestidge, C. A., Mc Phee, G., Rogers, M.-L.,
1110 Donoghue, J. F., Pillay, V., Johns, T. G., Kröger, N., Voelcker, N. H., 2015. Targeted drug delivery
1111 using genetically engineered diatom biosilica. *Nat. Commun.* 6: 8791.
1112
1113 De Riso, V., Raniello, R., Maumus, F., Rogato, A., Bowler, C., Falciatore, A., 2009. Gene silencing
1114 in the marine diatom *Phaeodactylum tricornutum*. *Nucleic Acids Res* 37, e96.
1115
1116 De Sanctis, S., Wenzler, M., Kroger, N., Malloni, W. M., Sumper, M., Deutzmann, R., Zadavec, P.,
1117 Brunner, E., Kremer, W., Kalbitzer, H. R., 2016. PSCD Domains of Pleuralin-1 from the Diatom
1118 *Cylindrotheca fusiformis*: NMR Structures and Interactions with Other Biosilica-Associated
1119 Proteins. *Structure* 24, 1178–1191.
1120
1121 De Stefano, L., Rendina, I., De Stefano, M., Bismuto, A., Maddalena, P., 2005. Marine diatoms as
1122 optical chemical sensors. *Appl. Phys. Lett.* 87: 233902.
1123
1124
1125 De Stefano, L., Rea, I., Rendina, I., De Stefano, M., Moretti, L., 2007. Lensless light focusing with
1126 the centric marine diatom *Coscinodiscus wailesii*. *Opt. Express* 15: 18082-18088.
1127
1128 De Stefano, L., Lamberti, A., Rotiroti, L., & De Stefano, M., 2008. Interfacing the nanostructured
1129 biosilica microshells of the marine diatom *Coscinodiscus wailesii* with biological matter. *Acta*
1130 *Biomater.*, 4(1), 126-130.
1131
1132 De Stefano, L., Maddalena, P., Moretti, L., Rea, I., Rendina, I., De Tommasi, E., Mocella, V., De
1133 Stefano, M., 2009. Nano-biosilica from marine diatoms: a brand new material for photonic
applications. *Superlattice. Microst.* 46: 84-89.

1134 De Stefano, L., De Stefano, M., De Tommasi, E., Rea, I., & Rendina, I., 2011. A natural source of
1135 porous biosilica for nanotech applications: the diatoms microalgae. *Phys. Status Solidi (c)*,
1136 8(6), 1820-1825.
1137

1138 De Tommasi, E., Rea, I., Mocella, V., Moretti, L., De Stefano, M., Rendina, I., De Stefano, L., 2010.
1139 Multi-wavelegth study of light transmitted through a single marine centric diatom. *Opt.*
1140 *Express* 18: 12203-12212.

1141 De Tommasi, E., De Luca, A. C., Lavanga, L., Dardano, P., De Stefano, M., De Stefano, L.,
1142 Langella, C., Rendina, I., Dholakia, K., Mazilu, M., 2014. Biologically enabled sub-diffractive
1143 focusing. *Opt. Express* 22: 27214-27227.

1144 De Tommasi, E., 2016. Light Manipulation by Single Cells: The Case of Diatoms. *J. Spectrosc.*,
1145 Article ID 2490128

1146 Di Caprio, G., Coppola, G., De Stefano, L., De Stefano, M., Antonucci, A., Congestri, R., De
1147 Tommasi, E., 2014. Shedding light on diatom photonics by means of digital holography. *J.*
1148 *Biophotonics* 7: 341-350.

1149 Durkin, C. A., Mock, T. & Armbrust, E., 2009. Chitin in diatoms and its association with the cell
1150 wall. *Eukaryot. Cell.* 8: 1038-1050.
1151

1152 Durkin, C. A., Marchetti, A., Bender, S. J., Truong, T., Morales, R., Mock, T. & Armbrust, E., 2012.
1153 Frustule-related gene tran-scription and the influence of diatom community composition on
1154 silica precipitation in an iron-limited environment. *Limnol. Oceanogr.* 57:1619-33.
1155

1156 Durkin, C. A., Kosster, J. A., Bender, S. J., Armbrust, E., 2016. The evolution of silicon
1157 transporters in diatoms. *J. Phycol.* 52, 716-731.

1158

1159 Falciatore, A., Casotti, R., Leblanc, C., Abrescia, C., Bowler, C., 1999. Transformation of
1160 nonselectable reporter genes in marine diatoms. *Mar. Biotechnol.* 1, 239–251.

1161

1162 Falkowski, P. G. and Raven, J. A., 2007. *Aquatic Photosynthesis Vol. 2*, Princeton University
1163 Press.

1164

1165 Ferrandez, A., 2017. Some variational problems on curves and applications. *Atlantis*
1166 *Transactions in Geometry*, 1, 199–222. [DOI](#)

1167

1168 Fang, Y., Chen, V. W., Cai, Y., Berrigan, J. D., Marder, S. R., Perry, J. W., Sandhage, K. H., 2012.
1169 Biologically Enabled Synthesis of Freestanding Metallic Structures Possessing Subwavelength
1170 Pore Arrays for Extraordinary (Surface Plasmon-Mediated) Infrared Transmission. *Adv.*
1171 *Funct. Mater.*, 22, 2550-2559.

1172

1173 Ferrara, M. A., Dardano, P., De Stefano, L., Rea, I., Coppola, G., Rendina, I., Congestri, R.,
1174 Antonucci, R., De Stefano, M., De Tommasi, E., 2014. Optical Properties of Diatom
1175 Nanostructured Biosilica *Arachnoidiscus* sp: Micro-Optics from Mother Nature, *Plos One* 9:
1176 e103750.

1177 Ferrara, M. A., De Tommasi, E., Coppola, G., De Stefano, L., Rea, I., Dardano, P., 2016. Diatom
1178 Valve Three-Dimensional Representation: A New Imaging Method Based on Combined
1179 Microscopies. *Int. J. Mol. Sci.* 17: 1645.

1180 Field, C. B., Behrenfeld, M. J., Randerson, J. T., Falkowski, P., 1998. Primary production of the
1181 biosphere: Integrating terrestrial and oceanic components. *Science* 281: 237-240.

1182 Finkel, Z. V., Kotrc, B, 2010. Silica Use Through Time: Macroevolutionary Change in the
1183 Morphology of the Diatom Frustule. *Geomicrobiol. J.* 27: 596-608.
1184

1185 Fischer, H., Robl, I., Sumper, M., Kröger, N., 1999. Targeting and covalent modification of cell
1186 wall and membrane proteins heterologously expressed in the diatom *Cylindrotheca*
1187 *fusiformis* (Bacillariophyceae). *J. Phycol.* 35:113–20;
1188

1189 Fougerolle, Y., Gielis, J., Truchetet, F., 2013. A robust evolutionary algorithm for the recovery
1190 of rational Gielis curves, *Pattern Recognition*, vol 46(8), 2078–2091.□
1191

1192 Forestiere, C., He, Y., Wang, R., Kirby, R. M., & Dal Negro, L., 2015. Inverse design of metal
1193 nanoparticles' morphology. *ACS Photonics*, 3(1), 68-78.
1194

1195 Friedrichs, L., Maier, M., Hamm, C., 2012. A new method for exact three-dimensional
1196 reconstructions of diatom frustules. *J. Micros.* 248: 208-217.
1197

1198 Frings, P. J., Clymans, W., Fontorbe G., De La Rocha . L. , Conley, D.J., 2016. The continental Si
1199 cycle and its impact on the ocean Si isotope budget. *Chem. Geol.* 425, 12–36.
1200

1201

1202 Fuhrmann, T., Landwehr, S., El Rharbi-Kucki, M., Sumper, M., 2004. Diatom as living photonic
1203 crystals. *Appl. Phys. B* 78: 257-260.

1204 Furukawa, T., Watanabe, M., Shihira-Ishikawa, I., 1998. Green- and blue-light-mediated
1205 chloroplast migration in the centric diatom *Pleurosira laevis*. *Protoplasma* 203: 214-220.

1206 Galachyants, Y.P., Zakharova, Y.R., Petrova, D.P., Morozov, A.A., Sidorov, I.A., Marchenkov, A.M.,

1207 Logacheva, M.D., Markelov, M.L., Khabudaev, K.V., Likhoshway, Y.V. et al. 2015. Sequencing of
1208 the complete genome of an araphid pennate diatom *Synedra acus* subsp. *radians* from Lake
1209 Baikal. Dokl Biochem Biophys, 461:84-88.

1210 Gale, D. K., Gutu, T., Jiao, J., Chang, C.-H., Rorrer, G. L., 2009. Photoluminescence Detection of
1211 Biomolecules by Antibody-Functionalized Diatom. Biosilica. Ad. Funct. Mater. 19: 926–933.
1212

1213 Gielis, J., 2003. A generic geometric transformation that unifies a large range of natural and
1214 abstract shapes. Am. J. Bot., 90(3), 333–338.
1215

1216 Gielis, J., Haesen S., & Verstraelen L., 2005. Universal shapes: from the supereggs of Piet Hein
1217 to the cosmic egg of George Lemaître. Kragujevac J. Mathematics, 28, 55–67. [\[2\]](#)
1218

1219 Gielis, J., Caratelli, D., Fougerolle, Y., Ricci, P.E., Gerats, T., 2011. Universal Natural Shapes:
1220 From unifying shape description to simple methods for shape analysis and boundary value
1221 problems. PLOS One. D-11-01115R2 10.1371
1222

1223 Gielis, J., 2017. Geometrical Beauty of Plants. Atlantis-Springer.
1224

1225 Gordon, R., Losic, D., Tiffany, M. A., Nagy, S. S. & Sterrenburg, F. A. S., 2009. The Glass
1226 Menagerie: diatoms for novel applications in nanotechnology. Trends Biotechnol. 27: 116-
1227 127.

1228 Gräb, O., Abacilar, M., Daus, F., Geyer A., Steinem C., 2016. 3D-Membrane Stacks on Supported
1229 Membranes Composed of Diatom Lipids Induced by Long-Chain Polyamines.
1230 Langmuir.32(39):10144-10152

1231 Greanya, V., 2016. Bioinspired Photonics: Optical Structures and Systems Inspired by Nature.

1232 CRC Press, Taylor and Francis Group.

1233 Gross, M., 2012. The mysteries of the diatoms. *Curr. Biol.* Vol 22 No 15.

1234 Hale, M. S., Mitchell, J. G., 2001. Functional morphology of diatom frustule microstructures:
1235 hydrodynamic control of Brownian particle diffusion and advection. *Aquat. Microb. Ecol.* 24:
1236 287-295.

1237

1238 Hale, M. S., Mitchell, J. G., 2002. Effects of Particle Size, Flow Velocity, and Cell Surface
1239 Microtopography on the Motion of Submicrometer Particles over Diatoms. *Nano Lett.* 2, 657-
1240 663.

1241 Hamm, C. E., Merkel, R., Springer, O., Jurkoj, P., Maier, C., Prechtel, K. & Smetacek, V., 2003.
1242 Architecture and material properties of diatom shells provide effective mechanical protection.
1243 *Nature* 421: 841-843.

1244

1245 Hamm, C., 2005. The evolution of advanced mechanical defenses and potential technological
1246 applications of diatom shells. *J. Nanosci. Nanotechnol.* 5: 108-119.

1247 Herringer, J., Dorrington, G., Rosengarten, G., 2014. Effective Diffusion Coefficient and Average
1248 Drift Velocity for a Bioinspired Drift Ratchet. *Proceedings of the Australian Fluid Mechanics*
1249 *Conference.*

1250 Hopes, A., Nekrasov, V., Kamoun, S., Mock, T. 2016. Editing of the urease gene by CRISPR-Cas
1251 in the diatom *Thalassiosira pseudonana*. *Plant Methods.* 24;12:49.

1252

1253 Hicks, Y. A., Marshall, D., Rosin, P. L., Martin, R. R., Mann, D. G., & Droop, S. J., 2006. A model of
1254 diatom shape and texture for analysis, synthesis and identification. *Mach. Vis. Appl.*, 17(5),

1255 297-307.

1256

1257 Hildebrand, M., Volcani, B. E., Gassmann, W. & Schroeder, J. I., 1997. A gene family of silicon
1258 transporters. *Nature* 385: 688–9.

1259

1260 Hildebrand, M., Dahlin, K. & Volcani, B. E., 1998. Characterization of a silicon transporter gene
1261 family in *Cylindrotheca fusiformis*: sequences, expression analysis, and identification of
1262 homologs in other diatoms. *Mol. Gen. Genet. MGG.* 260:480–6.

1263

1264 Hildebrand, M. 2008. Diatoms, biomineralization processes, and genomics. *Chem. Rev.*
1265 108:4855–74.

1266

1267 Hsu, S.H., Paoletti, C., Torres, M., Ritchie, R. J., Larkum, A. W. D., Grillet, C., 2012. Light
1268 transmission of the marine diatom *Coscinodiscus wailesii*. *Proc. SPIE* 8339, *Bioinspir.,*
1269 *Biomim., and Bioreplic.:* 83390F.

1270

1271 Huclova, S., Erni, D., & Fröhlich, J., 2010. Modelling effective dielectric properties of materials
1272 containing diverse types of biological cells. *J. of Phys. D: Appl. Phys.*, 43(36), 365405.

1273

1274 Huysmann, M.J.J., Vyverman, W., De Veylder, L., 2014. Molecular regulation of the diatom cell
1275 cycle. *J. Exp. Bot.* 65 (10): 2573-2584.

1276

1277 Javaheri, N., Dries, R., Kaandorp, J., 2014. Understanding the Sub-Cellular Dynamics of Silicon
1278 Transportation and Synthesis in Diatoms Using Population-Level Data and Computational
1279 Optimization. *PLOS Comput. Biol.* 10; 6, e1003687.

1280 Jeffryes, C., Gutu, T., Jiao, J., Rorrer, G. L., 2008. Two-stage photobioreactor process for the
1281 metabolic insertion of nanostructured germanium into the silica microstructure of the
1282 diatom *Pinnularia* sp. Mater. Sci. Eng. C 28, 107-118.

1283 Jeffryes, C., Gutu, T., Jiao, J., Rorrer, G. L., 2008bis. Metabolic Insertion of Nanostructured TiO₂
1284 into Patterned Biosilica of the Diatom *Pinnularia* sp. by a Two-Stage Bioreactor Cultivation
1285 Process. ACS Nano 2, 2103-2112.

1286

1287 Joannopoulos, J. D., Johnson S. G., Winn, J. N., Meade, R. D., 2008. Photonic Crystals: Molding
1288 the Flow of Light. Princeton University Press, 2nd Edition.

1289 Kammer, M., Hedric, R., Ehrlich, H., Popp, J., Brunner, E., Krafft, C., 2010. Spatially resolved
1290 determination of the structure and composition of diatom cell walls by Raman and FTIR
1291 imaging. Anal. Bioanal. Chem. 398: 509-517.

1292

1293 Karas, B.J., Diner, R.E., Lefebvre, S.C., McQuaid, J., Phillips, A.P., Noddings, C.M., Brunson, J.K.,
1294 Valas, R.E., Deerinck, T.J., Jablanovic, J., et al., 2015. Designer diatom episomes delivered by
1295 bacterial conjugation. Nat. Commun. 6:6925.

1296

1297 Katz, L. A., 2012. Origin and diversification of eukaryotes. Ann. Rev. Microbiol. 66: 411–427.

1298 Kay, M., 2008. Digital Diatoms, video exhibited at Ernst Haeckel Phyletic Museum.
1299 <https://vimeo.com/37370778>.

1300 Keeling, P.J. , Burki, F. , Wilcox, H.M., Allam, B., Allen, E.E., Amaral-Zettler, L.A., Armbrust, E.V.,
1301 Archibald, J.M., Bharti, A.K., Bell, C.J., et al. 2014. The Marine Microbial Eukaryote
1302 Transcriptome Sequencing Project (MMETSP): illuminating the functional diversity of
1303 eukaryotic life in the oceans through transcriptome sequencing. PLoS Biol, 12 , p. e1001889

1304

1305 Kettner, C., Reimann, P., Hänggi, P., Müller, 2000. Drift ratchet. *Phys. Rev. E* 61, 312-323.

1306 Kirk, J. T. O., 2011. *Light and Photosynthesis in Aquatic Ecosystems*. Cambridge University
1307 Press.

1308 Knight, M. J., Senior, L., Nancolas, B., Ratcliffe, S., Curnow, P., 2016. Direct evidence of the
1309 molecular basis for biological silicon transport. *Nat. Commun.* 7:11926

1310

1311 Koiso, M., Palmer, B., 2008. Equilibria for anisotropic energies and the Gielis Formula. *Forma*
1312 (Society for Science on Form, Japan), 23(1), 1–8.

1313

1314 Kolle, M., 2011. *Photonic structures inspired by nature*. Springer.

1315

1316 Kooistra, W. H. C. F., Medlin, L. K., 1996. Evolution of the diatoms (Bacillariophyta): IV. A
1317 reconstruction of their age from small subunit rRNA coding regions and the fossil record. *Mol.*
1318 *Phylogenet. Evol.* 6: 391–407.

1319

1320 Kooistra, W. H. C. F., Gersonde, R., Medlin, L. K. et al. , 2007 The origin and evolution of the
1321 diatoms: their adaptation to a planktonic existence. In Falkowski, P. G. and Knoll, A. H. (eds),
1322 *Evolution of Primary Producers in the Sea*, Elsevier Academic Press, Burlington, MA, pp. 207–
1323 249.

1324

1325 Kröger, N., Bergsdorf, C., Sumper, M., 1996. Frustulins: domain conservation in a protein
1326 family associated with diatom cell walls. *Eur. J. Biochem.* 15;239(2):259-64.

1327

1328 Kröger, N., Lehmann, G., Rachel, R., Sumper, M., 1997. Characterization of a 200-kDa diatom
1329 protein that is specifically associated with a silica-based substructure of the cell wall. *Eur. J.*
1330 *Biochem.* 250, 99–105.

1331

1332 Kröger, N., Deutzmann, R., Sumper, M., 1999. Polycationic peptides from diatom biosilica that
1333 direct silica nanosphere formation. *Science* 286, 1129–1132.

1334

1335 Kröger, N., Deutzmann, R., Sumper, M., 2001. Silica precipitating peptides from diatoms. The
1336 chemical structure of silaffin-A from *Cylindrotheca fusiformis*. *J. Biol. Chem.* 276, 26066–
1337 26070.

1338

1339 Kröger, N., Lorenz, S., Brunner, E., Sumper, M., 2002. Self-assembly of highly phosphorylated
1340 silaffins and their function in biosilica morphogenesis. *Science* 298: 584–586.

1341

1342 Kröger, N., Poulsen, N., 2007. Biochemistry and molecular genetics of silica biomineralization
1343 in diatoms. *Handbook of Biomineralization: Biological Aspects and Structure Formation.*
1344 Edited by: Baeuerlein E., Wiley-VCH, Weinheim, 43-58.

1345

1346 Kröger, N., Poulsen, N., 2008. Diatoms—From cell wall biogenesis to nanotechnology. *Annu.*
1347 *Rev. Genet.* 42:83–107

1348

1349 Kroth, P. G. 2007. Genetic transformation: a tool to study protein targeting in diatoms.
1350 *Methods Mol Biol* 390, 257-267

1351

1352 Kwon, S. Y., Park, S., Nichols, W. T., 2014. Self-assembled Diatom Substrates with Plasmonic
1353 Functionality. *J. Korean Phys. Soc.*, 64, 1179-1184.
1354

1355 Lamastra, F. R., De Angelis, R., Antonucci, A., Salvatori, D., Proposito, P., Casalboni, M.,
1356 Congestri, R., Melinoe, S., Nannia, F., 2014. Polymer composite random lasers based on diatom
1357 frustules as scatterers, *RSC Adv.* 4: 61809-61816.
1358

1359 Lechner C. C., Becker F. W. C., 2015. Silaffins in Silica Biomineralization and Biomimetic Silica
1360 Precipitation. *Mar Drugs.* 13(8): 5297-5333.
1361

1362 Legay, A., & Zilian, A., 2008. Enriched space-time finite elements for fluid-structure
1363 interaction. *European Journal of Computational Mechanics/Revue Européenne de Mécanique*
1364 *Numérique*, 17(5-7), 725-736.
1365

1366 Lin, S., et al., 2016. A geometrical model for testing bilateral symmetry of bamboo leaf with a
1367 simplified Gielis equation. *Ecol. Evol.* 6(19), 6798-6806.
1368

1369 Lommer, M., Specht, M., Roy, A., Kraemer, L., Andreson, R., Gutowska, M. A., Wolf, J., Bergner,
1370 S.V., Schilhabel, M.B., Klostermeier, U. C. *et al*, 2012. Genome and low-iron response of an
1371 oceanic diatom adapted to chronic iron limitation. *Genome Biol.* 13: R66.
1372

1373 Losic, D., Pillar, R. J., Dilger, T., Mitchell, J. G., Voelcker, N. H., 2007. Atomic force microscopy
1374 (AFM) characterization of the porous silica nanostructure of two centric diatoms. *J. Porous*
1375 *Mater.* 14: 61-69.

1376 Losic, D., Mitchell, J. G., Lal, R., Voelcker, N. H., 2007. Rapid Fabrication of Micro- and

1377 Nanoscale Patterns by Replica Molding from Diatom Biosilica. *Adv. Funct. Mater.* 17, 2439-
1378 2446.
1379

1380 Losic, D., Mitchell, J. G., Voelcker, N. H., 2009. Diatomaceous Lessons in Nanotechnology and
1381 Advanced Materials. *Adv. Mater.* 21: 2947-2958.

1382 Lu, J., Sun, C., Wang, Q. J., 2015. Mechanical Simulation of a Diatom Frustule Structure. *J. Bionic.*
1383 *Eng.* 12: 98-108.
1384

1385 Ma, J. F., Tamai, K., Yamaji, N., Mitani, N., Konishi, S., Katsuhara, M., Ishiguro, M. et al. 2006. A
1386 silicon transporter in rice. *Nature* 440:688–91.
1387

1388 Ma, J. F., Yamaji, N., Mitani, N., Tamai, K., Konishi, S., Fujiwara, T., Katsuhara, M. et al. 2007. An
1389 efflux transporter of silicon in rice. *Nature* 448:209–12.
1390

1391 Macías, D., Adam, P. M., Ruíz-Cortés, V., Rodríguez-Oliveros, R., & Sánchez-Gil, J. A., 2012.
1392 Heuristic optimization for the design of plasmonic nanowires with specific resonant and
1393 scattering properties. *Opt. Express* 20(12), 13146-13163.
1394

1395 Maldonado, M., Carmona, M. C., Uriz, M. J., Cruzado, A., 1999. Decline in Mesozoic reef-building
1396 sponges explained by silicon limitation. *Nature* 401:785–8.
1397

1398 Mann, D.G., Vanormelingen, P., 2013. An inordinate fondness? The number, distributions, and
1399 origins of diatom species. *J. Eukaryot. Microbiol.* 60(4):414–420. 5
1400

1401 Marron, A. O., Alston, M. J., Heavens, D., Akam, M., Caccamo, M., Holland, P. W. H. & Walker, G.

1402 2013. A family of diatom-like silicon transporters in the siliceous loricate choanoflagellates.
1403 Proc. R. Soc. Lond. Biol. Sci. 280:20122543.
1404
1405 Martin-Jezequel, V., Hildebrand, M. & Brzezinski, M. A., 2000. Silicon metabolism in diatoms:
1406 implications for growth. J. Phycol. 36:821–40.
1407
1408 Matsukizono, H, Jin, R. H., 2012. High-temperature-resistant chiral silica generated on chiral
1409 crystalline templates at neutral pH and ambient conditions. Angew Chem Int Ed Engl 51(24):
1410 5862-5.
1411
1412 Matsuura, M., 2015. Gielis' superformula and regular polygons. J. Geometry 106 (2), 1–21.
1413
1414 Matthias, S., Müller, 2003. Asymmetric pores in a silicon membrane acting as massively
1415 parallel brownian ratchets. Nature 424: 53-57.
1416
1417 Miklasz, K. A., Denny, M. W., 2010. Diatom sinking speeds: Improved predictions and insight
1418 from a modified Stokes' law. Limnol. Oceanogr. 55: 2513-2525.
1419 Mock, T., Samanta, M.P., Iverson, V., Berthiaume, C., Robison, M., Holtermann, K., Durkin, C.A.,
1420 BonDurant, S.S., Richmond, K., Rodesch, M., Kallas, T., Huttlin, E.L., Cerrina, F., Sussmann, M.R.,
1421 Armbrust, E.V., 2008. Whole-genome expression profiling of the marine diatom *Thalassiosira*
1422 *pseudonana* identifies genes involved in silicon bioprocesses. Proc. Natl. Acad. Sci. U. S. A. 105,
1423 1579–1584.
1424
1425 Mock, T., Otilar, R. P., Strauss, J., McMullan, M., Paajanen, P., Schmutz, J., Salamov A., Sanges,
1426 R., Toseland, A. , Ward, Ben J. Allen, A., E. Dupont, C. L., Frickenhaus, S., Maumus, F., Veluchamy,

1427 A., Wu, T., Barry, K. W., Falciatore, A., Ferrante, M. I., Fortunato, A. E., Glöckner, G., Gruber, A.,
1428 Hipkin, R., Janech, M. G., Kroth, P. G., Leese, F., Lindquist, E. A., Lyon, B. R., Martin, J., Mayer, C.,
1429 Parker, M., Quesneville, H., Raymond, J. A., Uhlig, C., Valas, R. E., Valentin, K. U., Worden, A. Z.,
1430 Armbrust, E. V., Clark, M. D., Bowler, C., Green, B. R., Moulton, V., van Oosterhout, C. &
1431 Grigoriev I. V., 2017. Evolutionary genomics of the cold-adapted diatom *Fragilariopsis*
1432 *cylindrus*. Nature, 541, 536-540.

1433

1434 Moreno, M. D., Ma, K., Schoenung, J., Davila, L. P., 2015. An integrated approach for probing the
1435 structure and mechanical properties of diatoms: Toward engineered nanotemplates. Acta
1436 Biomater. 25: 313-324.

1437 Muhseen, Z.T., Xiong, Q., Chen, Z., Ge, F. 2015. Proteomics studies on stress responses in
1438 diatoms. Proteomics 15(23-24):3943-53.

1439

1440 Natalini, P., Patrizi, R., & Ricci, P. E., 2008. The Dirichlet problem for the Laplace equation in a
1441 starlike domain of a Riemann surface. Numerical Algorithms 49(1-4), 299-313.

1442

1443 Natalini, P., Patrizi, R., & Ricci, P. E., 2009. Heat problems for a starlike shaped plate. Appl.
1444 Math. Comput. 215(2), 495-502.

1445

1446 Nelson, D. M., Treguer, P., Brezinski, M. A., Leynaert, A., Queguiner, B., 1995. Production and
1447 dissolution of biogenic silica in the ocean - revised global estimates, comparison with regional
1448 data and relationship to biogenic sedimentation. Glob. Biogeochem. Cycles 9, 359-372.

1449

1450 Niklas, K.J., 2004. Plant allometry: is there a grand unifying theory? *Biological reviews*, 79(04),
1451 871-889.

1452

1453 Niklas, K. J., & Kutschera, U., 2016. From Goethe's plant archetype via Haeckel's biogenetic law
1454 to plant evo-devo. *Theory in Biosciences*, 1-9.

1455

1456 Niu, Y.F., Yang, Z.K., Zhang, M.H., Zhu, C.C., Yang, W.D., Liu, J.S., Li, H.Y., 2012. Transformation
1457 of diatom *Phaeodactylum tricornutum* by electroporation and establishment of inducible
1458 selection marker. *Biotechniques* 52.

1459

1460 Noyes, J., Sumper, M., Vukusic, P., 2008. Light manipulation in a marine diatom. *J. of Mater.*
1461 *Res.* 23: 3229-3235.

1462

1463 Okita, T.W., Volcani, B.E., 1980. Role of silicon in diatom metabolism: X. Polypeptide labelling
1464 patterns during the cell cycle, silicate starvation and recovery in *Cylindrotheca fusiformis*.
1465 *Exp. Cell. Res.* 125, 471-481.

1466

1467 Oren, A., 1999. The enigma of square and triangular halohilic Archaea. *Enigmatic*
1468 *Microorganisms and Life in Extreme Environments*, 339-355.

1469

1470 Pahlow, M., Riebesell, U., Wolf-Gladrow, D. A., 1997. Impact of cell shape and chain formation
1471 on nutrient acquisition by marine diatoms. *Limnol. Oceanogr.* 42: 1660-1672.

1472

1473 Pamirsky, E., Golokhvast, K.S., 2013 Silaffins of diatoms: from applied biotechnology to
1474 biomedicine. *Mar. Drugs.* 11(9), 3155-67.

1475 Pan, Z., Lerch, S. J. L., Xu, L., Li, X., Cguang, Y.-J., Howe, J. Y., Mahurin, S. M., Dai, S. & Hildebrand,
1476 M., 2014. Electronically transparent graphene replicas of diatoms: a new technique for the
1477 investigation of frustule morphology. *Sci. Rep.* 4: 6117.

1478 Parashchenko, M. A., Filippov, N. S., Kirienko, V. V., & Romanov, S. I., 2014. Electroosmotic
1479 pump based on asymmetric silicon microchannel membranes. *Optoelectronics,*
1480 *Instrumentation and Data Processing* 50(3), 315-322.

1481

1482 Parker, A. R., Townley, H. E., 2007. Biomimetics of photonic nanostructures. *Nat. Nanotech.* 2:
1483 347-353.

1484 Payne, E. K., Rosi, N. L., Xue, C., Mirkin, C. A. , 2005. Sacrificial Biological Templates for the
1485 Formation of Nanostructured Metallic Microshells. *Angew. Chem. Int. Edit.*, 44, 5064-5067.

1486 Pickett-Heaps, J., Schmid, A.M.M., Edgar, L.A., 1990. The cell biology of diatom valve formation.
1487 *Progr. Phycol. Res.* 7: 1-168.

1488

1489 Pondaven, P., Gallinari, M., Chollet, S., Bucciarelli, E., Sarthou, G., Schultes, S., Jean, F., 2007.
1490 Grazing-induced Changes in Cell Wall Silicification in a Marine Diatom. *Protist* 158: 21-28.

1491

1492 Poulsen, N., Kröger, N., 2004. Silica morphogenesis by alternative processing of silaffins in the
1493 diatom *Thalassiosira pseudonana*. *J. Biol. Chem.* 279:42993-42999.

1494

1495 Poulsen, N., Kröger, N., 2005. A new molecular tool for transgenic diatoms-control of mRNA
1496 and protein biosynthesis by an inducible promoter-terminator cassette. *FEBS J.* 272:3413-23
1497

1498 Poulsen, N., Chesley, P.M., Kröger, N., 2005. Molecular genetic manipulation of the diatom

1499 *Thalassiosira pseudonana* (Bacillariophyceae). J. Phycol. 42, 1059–1065.

1500

1501 Poulsen, N., Scheffel, A., Sheppard, V.C., Chesley, P.M., Kröger, N., 2013. Penatlysine clusters
1502 mediate silica targeting of silaffins in *Thalassiosira pseudonana*. J. Biol. Chem. 12; 288(28):
1503 20100–20109.

1504

1505 Qi, M., Lidorikis, E., Rakich, P. T., Johnson, S. G., Joannopoulos, J. D., Ippen, E. P., Smith, H. I.,
1506 2004. A three-dimensional optical photonic crystal with designed point defects. Nature 429:
1507 538-542.

1508

1509 Qin, T.; Gutu, T.; Jiao, J.; Chang, C.-H., Rorrer, G. L., 2008. Photoluminescence of Silica
1510 Nanostructures from Bioreactor Culture of Marine Diatom *Nitzschia frustulum*. J. Nanosci.
1511 Nanotechno. 8: 2392-2398.

1512 Rastogi, A., Murik, O., Bowler, C., Tirichine, L., 2016. PhytoCRISP-Ex: a web-based and stand-
1513 alone application to find specific target sequences for CRISPR/CAS editing. BMC Bioinfo. 17:
1514 261.

1515 Ren, F, Campbell, J., Rorrer, G. L., Wang, A. X., 2014. Surface-Enhanced Raman Spectroscopy
1516 Sensors From Nanobiosilica With Self-Assembled Plasmonic Nanoparticles. IEEE J. Sel. Top.
1517 Quant., 20, 6900806.

1518 Richthammer, P., Börmel, M., Brunner, E., van Pée, K.H., 2011. Biomineralization in diatoms:
1519 The role of silacidins. Chembiochem. 12(9):1362–1366.

1520

1521 Romann, J., Valmalette, J.-C., Royset, A., Einarsud, M.-A., 2015. Optical properties of single
1522 diatom frustules revealed by confocal microspectroscopy. Opt. Lett. 40: 740-743.

1523

1524 Romann, J., Valmalette, J.-C., Skogen Chauton, M., Tranell, G., Einarsud, M.-A., Valdstein, O.
1525 2015. Wavelength and orientation dependent capture of light by diatom frustule
1526 nanostructures. Sc. Rep. 5: 17403.

1527 Round, F. E., Crawford, R. M., Mann, D. G., 1990. The diatoms. Biology and morphology of the
1528 genera. Cambridge University Press.

1529

1530 Sabatino, V., Russo, M.T., Patil, S., d'Ippolito, G., Fontana, A., Ferrante, M.I., 2015. Establishment
1531 of Genetic Transformation in the Sexually Reproducing Diatoms *Pseudo-nitzschia multistriata*
1532 and *Pseudo-nitzschia arenysensis* and Inheritance of the Transgene. Mar Biotechnol
1533 17(4):452-62

1534

1535 Scheffel, A., Poulsen, N., Shian, S., Kröger, N., 2011. Nanopatterned protein microrings from a
1536 diatom that direct silica morphogenesis. Proc. Natl Acad. Sci. USA 108, 3175–3180.

1537

1538 Shi, P.-J., et al., 2015. Capturing spiral growth of conifers using superellipse to model tree-ring
1539 geometric shape. Front. Plant Sci., 6, 856.

1540

1541 Schroder, H.C., Perovi-Ottstadt, S., Rothenberger, M., Wiens, M., Schwertner, H., Batel, R.,
1542 Korzhev, M. et al., 2004. Silica transport in the demosponge *Suberites domuncula*:
1543 fluorescence emission analysis using the PDMPO probe and cloning of a potential transporter.
1544 Biochem. J. 381:665–73.

1545

1546 Shihira-Ishikawa, I., Nakamura, T., Higashi, S., Watanabe, M., 2007. Distinct Responses of
1547 Chloroplasts to Blue and Green Laser Microbeam Irradiations in the Centric Diatom *Pleurosira*

1548 *laevis*. Photochem. Photobiol. 83: 1101-1109

1549

1550 Shrestha, R.P., Hildebrand, M., 2015. Evidence for a regulatory role of diatom silicon
1551 transporters in cellular silicon responses. Eukaryotic Cell 14: 29–40.

1552

1553 Shrestha, P.R., Tesson, B., Norden-Krichmar, T., Federowicz, S., Hildebrand, M., Allen, A. E.
1554 2012. Whole transcriptome analysis of the silicon response of the diatom *Thalassiosira*
1555 *pseudonana*. BMC Genomics 13:499

1556

1557 Simó, R., 2001. Production of atmospheric sulfur by oceanic plankton: biogeochemical,
1558 ecological and evolutionary links. Trends Ecol. Evol. 16: 287-294.

1559

1560 Smayda, T. J., 1970. The suspension and sinking of phytoplankton in the sea. Oceanogr. Mar.
1561 Biol.: Ann. Rev. 8: 353-414.

1562 Smith, S.R., Glé, C., Abbriano, R.M., Traller, J.C., Davis, A., Trentacoste, E., Vernet, M., Allen,
1563 A.E., Hildebrand, M., 2016.
1564 Transcript level coordination of carbon pathways during silicon starvation
1565 induced lipid accumulation in the diatom *Thalassiosira pseudonana*. New Phytol. 210(3):890-
1566 904.

1567 Soler, C., Claquin, P., Goutx, M., Ragueneau, O., Moriceau, B., 2010. Impact of nutrient
1568 starvation on the biochemical composition of the marine diatom *Thalassiosira weissflogii*:
1569 from the whole cell to the frustule fraction. Biogeosciences Discuss., 7, 5953–5995.

1570

1571 Srajer, J., Majlis, B. Y., Gebeshuber, I. C., 2009. Microfluidic simulation of a colonial diatom
1572 chain reveals oscillatory movement. Acta Bot. Croat. 68: 431-441.

1573 Stec, K.F., Caputi, L., Buttigieg, P.L., D'Alelio, D., Ibarbalz, F.M., Sullivan, M.B., Chaffron, S.,
1574 Bowler, C., Ribera d'Alcalà, M., Iudicone, D. 2017. Modelling plankton ecosystems in the meta-
1575 omics era. Are we ready? *Mar Genomics* 32:1-17.

1576 Sumper, M., Kröger N., 2004. Silica formation in diatoms: The function of long-chain
1577 polyamines and silaffins. *J. Mater. Chem.* 14:2059–2065.

1578

1579 Sumper, M., Brunner, E., 2006. Learning from diatoms: Nature's tools for the production of
1580 nanostructured silica. *Adv. Funct. Mater.* 16:17–26.

1581

1582 Sumper, M., Brunner, E., 2008. Silica biomineralization in diatoms: the model organism
1583 *Thalassiosira pseudonana*. *Chembiochem.* 9: 1187-1194. 10.1002/cbic.200700764.

1584

1585 Svetličić, V., Žutić, V., Pletikapić, G., Radić, T. M., 2013. Marine Polysaccharide Networks and
1586 Diatoms at the Nanometric Scale. *Int. J. Mol. Sci.* 14: 20064-20078.

1587

1588 Tanaka, A., De Martino, A., Amato, A., Montsant, A., Mathieu, B., Rostaing P., Tirichine, L.,
1589 Bowler, C., 2014. Ultrastructure and Membrane Traffic During Cell Division in the Marine
1590 Pennate Diatom *Phaeodactylum tricornutum*. *Protist* 166, 5: 506-521.

1591

1592 Tanaka, T., Maeda, Y., Veluchamy, A., Tanaka, M., Abida, H., Maréchal, E., Bowler, C., Muto, M.,
1593 Sunaga, Y., Tanaka, M. et al, 2015. Oil accumulation by the oleaginous diatom *Fistulifera*
1594 *solaris* as revealed by the genome and transcriptome. *The Plant Cell* 27: 162–172.

1595

1596 Tassadit, A., Macías, D., Sanchez-Gil, J. A., Adam, P. M., & Rodriguez-Oliveros, R., 2011. Metal
1597 nanostars: Stochastic optimization of resonant scattering properties. *Superlattice Microst.*

1598 49(3), 288-293.

1599

1600 Terracciano, M., Shahbazi, M.-A., Correia, A., Rea, I., Lamberti, A., De Stefano, L., Santos, H. A.,
1601 2015. Surface bioengineering of diatomite based nanovectors for efficient intracellular uptake
1602 and drug delivery. *Nanoscale* 7: 20063–20074.

1603

1604 Thamatrakoln, K., Hildebrand, M., 2007. Analysis of *Thalassiosira pseudonana* silicon
1605 transporters indicates distinct regulatory levels and transport activity through the cell
1606 cycle. *Eukaryot. Cell* 6: 271–279.

1607

1608 Thamatrakoln, K., Alverson, A. J. & Hildebrand, M., 2006. Comparative sequence analysis of
1609 diatom silicon transporters: toward a mechanistic model of silicon transport. *J. Phycol.*
1610 42:822–34.

1611

1612 Thompson D'Arcy W., 1917. *On Growth and Form*. U.K., Cambridge: Cambridge University
1613 Press.☐

1614

1615 Toster, J., Iyer, K. S., Xiang, W., Rosei, F., Spiccia, L., Raston, C. L., 2013. Diatom frustules as
1616 light traps enhance DSSC efficiency. *Nanoscale* 5: 873-876.

1617

1618 Townley, H. E., 2011. *Diatom frustules: physical, optical and biotechnological applications*.
1619 *The diatom world*, Springer, ISBN 978-94-007-1327-7

1620

1621 Trainer, V.L., Bates, S.S., Lundholm, N., Thessen, A.E., Cochlan, W.P., Adams, N.G., Trick, C.G.,
1622 2012. *Pseudo-nitzschia* physiological ecology, phylogeny, toxicity, monitoring and impacts on

1623 ecosystem health. Harmful Algae 14, 271–300.

1624

1625 Traller, J.C., Cokus, TokusLopez, D. A., Gaidarenko, O., Smith, S, R., McCrow, J. P. Gallaher,
1626 S.D., Podell, S., Thompson, M., Cook, O., Morselli, M., Jaroszewicz, A., Allen, E. E., Allen, A.E.,
1627 Merchant, S.S., Pellegrini, M. and Hildebrand M. 2016. Genome and methylome of the
1628 oleaginous diatom *Cyclotella cryptica* reveal genetic flexibility toward a high lipid phenotype.
1629 Biotechnol Biofuels 20169:258

1630

1631 van de Poll, W. H., Vrieling, E. G. & Gieskes, W. W. C., 1999. Location and expression of
1632 frustulins in the pennate diatoms *Cylindrotheca fusiformis*, *Navicula pelliculosa*, and *Navicula*
1633 *salinarum* (Bacillariophyceae). J. Phycol. 35:1044–53.

1634

1635 Volcani, B. E., 1981. Cell wall formation in diatoms: morphogenesis and biochemistry. Silicon
1636 and Siliceous Structures in Biological Systems, Springer , T. L. Simpson and B. E. Volcani (Eds).
1637

1638 Vukusic, P., Sambles, J. R., 2003. Photonic structures in biology. Nature 424: 852-855.

1639 Waite, A., Fisher, A., Thompson P. A., Harrison, P. J., 1997. Sinking rate versus cell volume
1640 relationships illuminate sinking rate control mechanisms in marine diatoms. Mar. Ecol. Prog.
1641 Ser. 157: 97-108.

1642 Wang, H., 2008. Investigation of trajectories of inviscid fluid particles in two-dimensional
1643 rotating boxes. Theoretical and Computational Fluid Dynamics, 22(1), 21-35.

1644

1645 Wang, C., Yu, S., Chen, W., Sun, C., 2013. `Highly Efficient Light-Trapping Structure Design
1646 Inspired By Natural Evolution. Sci. Rep. 3: 1025.

1647

1648 Wenzl, S., Hett, R., Richthammer, P., Sumper, M., 2008. Silacidins: highly acidic
1649 phosphopeptides from diatom shells assist in silica precipitation in vitro. *Angew. Chem.* 47,
1650 1729–1732.

1651 Weyman, P.D., Beerli, K., Lefebvre, S.C., Rivera, J., McCarthy, J.K., Heuberger, A.L., Peers, G.,
1652 Allen, A.E., Dupont, C.L., 2014. Inactivation of *Phaeodactylum tricornutum* urease gene using
1653 transcription activator-like effector nuclease-based targeted mutagenesis. *Plant Biotechnol J.*
1654

1655 Wilken, S., Hoffmann, B., Hersch, N., Kirchgessner, N., Dieluweit, S., Rubner, W., Hoffmann, L.J.,
1656 Merkel, R., Peeken I., 2011. Diatom frustules show increased mechanical strength and altered
1657 valve morphology under iron limitation. *Limnol. Oceanogr.* 56(4), 1399–1410
1658

1659 Zarghooni, B., Dadgarpour, A., Pourahmadazar, J., & Denidni, T. A., 2015. Supershaped
1660 metamaterial unit-cells using the Gielis formula. In *IEEE Antennas and Propagation Society,*
1661 *AP-S International Symposium (Digest)* (pp. 458–459).

1662 Zhou, S., Townsend, S., Xie, Y. M., Huang, X., Shen, J., & Li, Q., 2014. Design of fishnet
1663 metamaterials with broadband negative refractive index in the visible spectrum. *Optics*
1664 *letters*, 39(8), 2415-2418
1665